Tutorial

Quantum Master Equations: Tips and Tricks for Quantum Optics, Quantum Computing, and Beyond

Francesco Campaioli,[1,2,3,4,*] Jared H. Cole,[1,2,†] and Harini Hapuarachchi[1,2,‡]

[1] *Chemical and Quantum Physics, and ARC Centre of Excellence in Exciton Science*
[2] *School of Science, RMIT University, Melbourne 3000, Australia*
[3] *Dipartimento di Fisica e Astronomia "G. Galilei", Università degli Studi di Padova, I-35131 Padua, Italy*
[4] *Padua Quantum Technologies Research Center, Università degli Studi di Padova, I-35131 Padua, Italy*

(Received 19 May 2023; revised 31 January 2024; published 10 June 2024)

Quantum master equations are an invaluable tool to model the dynamics of a plethora of microscopic systems, ranging from quantum optics and quantum information processing to energy and charge transport, electronic and nuclear spin resonance, photochemistry, and more. This tutorial offers a concise and pedagogical introduction to quantum master equations, accessible to a broad, cross-disciplinary audience. The reader is guided through the basics of quantum dynamics with hands-on examples that increase in complexity. The tutorial covers essential methods such as the use of the Lindblad master equation, Redfield relaxation, and Floquet theory, as well as techniques such as Suzuki-Trotter expansion and numerical approaches for sparse solvers. These methods are illustrated with code snippets implemented in PYTHON and other languages, which can be used as a starting point for generalization and more sophisticated implementations.

DOI: 10.1103/PRXQuantum.5.020202

CONTENTS

*Corresponding author: francesco.campaioli@unipd.it
†Corresponding author: jared.cole@rmit.edu.au
‡Corresponding author: harini.hapuarachchi@rmit.edu.au

I. INTRODUCTION

Master equations are differential equations used to model the dynamics of systems that can be described as a probabilistic combination of some states. For example, the concentration dynamics of a chemical reaction $x \rightleftharpoons y$, where some reactants x lead to some products y, can be described by the differential equations

$$\begin{cases} \dot{p}_x = k_{y\to x} p_y - k_{x\to y} p_x, \\ \dot{p}_y = k_{x\to y} p_x - k_{y\to x} p_y, \end{cases} \tag{1}$$

where p_i represent the concentrations of species $i = x, y$, with $\dot{p}_i = dp_i/dt$ being their time derivative, and $k_{i\to j}$ represent the rates of the transitions from species i to species j. This equation can be easily solved to obtain the transient and steady-state concentrations of the reactants and products, as a function of their initial concentrations and transition rates. In a reaction such as the one modeled in Eq. (1), the total concentration is conserved, since $\dot{p}_{\text{tot}} := \dot{p}_x + \dot{p}_y = 0$. Then, by recasting the problem in terms of relative concentrations $p_i \to p_i/p_{\text{tot}}$, we can interpret p_i as *the probability of being in state i*. We can generalize this idea to formulate master equations as first-order differential equations to the vector of probabilities $\mathbf{p} = (p_1, \ldots, p_n)$ of being in one of the n states of some system of interest. As a result, the dynamics of the state probabilities are prescribed by the master equation

$$\dot{\mathbf{p}} = \mathbf{F}(\mathbf{p}, t), \tag{2}$$

with $\mathbf{F}$ often being a linear function of $\mathbf{p}$ represented by some generating matrix A, as in $\dot{\mathbf{p}} = A\mathbf{p}$.

However, when dealing with quantum systems, we must take into account that coherent superpositions of states participate in the evolution, as prescribed by Schrödinger's equation

$$\frac{d}{dt}|\psi(t)\rangle = -\frac{i}{\hbar} H |\psi(t)\rangle, \tag{3}$$

where H is the Hamiltonian of the system and $|\psi(t)\rangle = \sum_{j=1}^{n} c_j(t)|\phi_j\rangle$ is its state at time t, expressed as a coherent superposition of the eigenstates $\mathcal{B}_H = \{|\phi_i\rangle, \ldots, |\phi_n\rangle\}$ of the Hamiltonian, via the normalized complex coefficients $c_j(t)$ satisfying $\sum_i |c_i(t)|^2 = 1$. In this case, a vector of probabilities $\mathbf{p}$, with $p_i = |c_i|^2$, is no longer sufficient to completely describe the dynamics of the system, since different phases of c_i will lead to different solutions. Master equations for the dynamics of quantum systems can then be expressed by use of another representation of the state of the system, known as the density operator ρ. As discussed in detail in Sec. II, the density operator contains all the information regarding the probabilities (known as *populations*) of being in each state i, given by $p_i = \langle\phi_i|\rho|\phi_i\rangle$, as well as the phases (known as *coherences*) $\varphi_{ij} = \langle\phi_i|\rho|\phi_j\rangle$ associated with the coherent superpositions between basis states $|\phi_i\rangle$ and $|\phi_j\rangle$. Quantum master equations (QMEs) are then formulated by generalization of Eq. (2), as first-order differential equations to the density operator,

$$\dot{\rho} = \mathcal{F}(\rho, t). \tag{4}$$

In this tutorial we primarily cover a specific type of linear QME, one that respects a set of requirements for the evolution of the density operator, as discussed in Sec. III.

QMEs, initially developed in quantum optics to study light-matter interactions [1], have been used in a multitude of settings, across different disciplines and fields, such as photochemistry [2–4], energy and charge transport [5–7], high-precision magnetometry [8–10], electronic spin resonance [11–14] and nuclear spin resonance [15–17], quantum information processing [18–21], and thermodynamics in the quantum regime [22–24], and are certainly not limited to these settings. One of the key aspects of QMEs is that they provide a coarse-grained stochastic description [25] of the effect of unknown and uncontrollable agents on a system of interest [26], leading to a computationally inexpensive ensemble-averaged picture of the dynamics of quantum systems. QMEs can be phenomenological [27] or derived, from first principles [26], from a microscopic

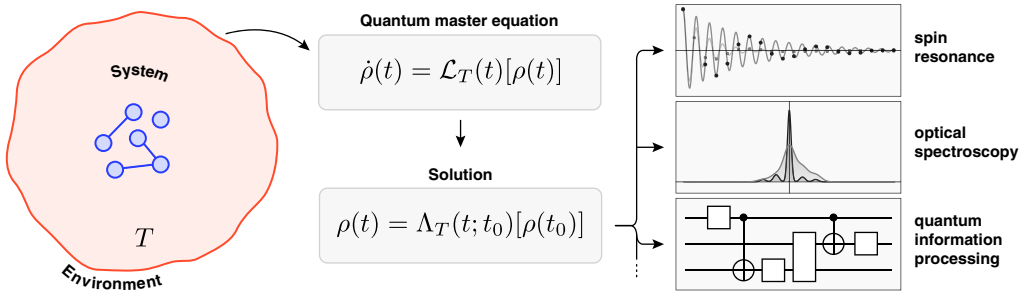

FIG. 1. QMEs provide a coarse-grained prescription for the dynamics of a quantum system (blue) that interacts weakly with its environment (red). The state ρ of the quantum system, represented by the density operator (see Sec. II), evolves according to some master equation $\dot{\rho}(t) = \mathcal{L}_T(t)[\rho(t)]$, where the Liouville superoperator $\mathcal{L}_T(t)$ generating the evolution may depend on time t and on the temperature T of the environment. The solution $\rho(t) = \Lambda_T(t;t_0)[\rho(t_0)]$ (and the master equation itself) can be used to study the steady-state and nonequilibrium properties of the system. QMEs are a staple tool for modeling spin resonance, optical spectra, and quantum information processing, and their use is certainly not limited to these fields and applications.

model of the system-environment interactions, as done in Sec. IV. They can be used to obtain qualitative trends [28] or make quantitatively accurate predictions [10]. They are just as suitable for the derivation of analytical results [2] as they are for the numerical simulation of complex systems with a large number of degrees of freedom [29]. For these reasons, QMEs, illustrated in Fig. 1, have become a standard approach to model the dynamics of quantum systems, and they have become a starting point for the formulation of more sophisticated descriptions.

Quantum master equations are now more accessible than ever, thanks to the many dedicated libraries and software packages, such as QUTIP [30], HOQST [31], SPINACH [32], and QOTOOLBOX, to name a few. These resources offer an invaluable platform for the quick implementation of models and their systematic exploration. Indeed, they have established themselves as a staple tool on the workbench of a vast community of researchers. Pedagogical tutorials and documentations of these libraries are just as precious as the software itself, offering an accessible starting point and a pathway for rapid progression.

Nevertheless, when one is directing newcomers from different research areas to QMEs, an obstacle is often presented by the vast and technical library of resources such as textbooks and notes, written for a specialized audience, which may not be ideal for cross-disciplinary readers. To bridge this gap, this tutorial provides the reader with a concise introduction to quantum master equations, with a pedagogical, hands-on approach, in the style of an interactive lesson or a workshop. The aim is to provide a handbook for third-year students joining the research group, master students ready to implement models, and doctoral students and cross-disciplinary researchers looking to consolidate and expand their expertise.

In this tutorial we cover essential theories, such as the Lindblad master equation, Bloch-Redfield theory, and Floquet theory, as well as numerical techniques for their solutions, such as the stochastic wave function method, the Suzuki-Trotter expansion, and numerical approaches for sparse matrices. We illustrate these methods using scripts implemented in PYTHON. Increasing in complexity, these examples aim to provide a deeper understanding of the methods implemented behind the curtains in libraries such as QUTIP and QOTOOLBOX, and can be used as a starting point for generalizations. This offers a unique opportunity to learn about numerical implementations and computational complexity as the methods are introduced. All the scripts included in the tutorial are available in Supplemental Material [33] and on GitHub, in the repository `qme`. Versions of these scripts in MATLAB and MATHEMATICA can also be found in Supplemental Material [33].

II. DENSITY OPERATORS

In this section we briefly review the mathematical description of the *state* of a quantum system, focusing on the numerical implementation of state vectors and density operators. We assume that the reader is familiar with the *postulates of quantum mechanics*, Hilbert spaces, expectation values, time evolution, and composite systems, which can be reviewed in Refs. [26,34–41].

A. Pure states

Let us consider a d-dimensional quantum system with Hilbert space $\mathcal{H}$. Let $\mathcal{B} := \{|\phi_1\rangle, |\phi_2\rangle, \ldots, |\phi_d\rangle\}$ be an orthonormal basis for $\mathcal{H}$, so that $\langle\phi_i|\phi_j\rangle = \delta_{ij}$. For example, $\mathcal{B}$ could be given by the orthonormal eigenstates of a Hermitian operator such as some Hamiltonian H. Any state of the system can be expressed as a *coherent superposition* with complex coefficients $c_i \in \mathbb{C}$,

$$|\psi\rangle = c_1|\phi_1\rangle + c_2|\phi_2\rangle + \cdots + c_d|\phi_d\rangle = \sum_{j=1}^{d} c_j|\phi_j\rangle, \quad (5)$$

where the coefficients c_j are such that $\langle\psi|\psi\rangle = \sum_{j=1}^{d} |c_j|^2 = 1$, according to the Born interpretation of the wave function [42]. The square of the coefficients in Eq. (5), $|c_j|^2$, represents the probability of finding the system in the eigenstate $|\phi_j\rangle$ upon measurement in the considered basis $\mathcal{B}$. See Ref. [34] for a review of projective measurement and Ref. [41] for the generalization to positive operator–valued measures).

Unit vectors such as $|\psi\rangle$ are called "pure states." A pure state contains all the available physical information about the system, such as the expectation value of an observable $\mathcal{A}$ associated with Hermitian operator A,

$$\langle A\rangle = \langle\psi|A|\psi\rangle. \tag{6}$$

The PYTHON script B.1 in Supplemental Material [33] uses methods from the NUMPY library to implement state vectors and operators, and to calculate the expectation value of some observable.

B. Mixed states: Proper and improper mixtures

There are two important scenarios where pure states are no longer sufficient to describe the state of a system. First, in experimental settings, we often lack knowledge of the exact pure state $|\psi\rangle$ of our system. Instead, we may know that the system is in any of the pure orthonormal states $\{|\psi_j\rangle\}$ with some probabilities $\{p_j\}$. In other words, our knowledge of the system is represented by a *statistical mixture of pure states*, described by the set $\{|\psi_j\rangle, p_j\}$. In such a case, when more than one p_j is nonzero, the system is said to be in a *mixed state*. This is sometimes referred to as a *proper* mixture [43]. In spin echo experiments [44], the average state of a large number of independent spins is typically interpreted as a proper mixture. Averaging over many realizations of the same stochastic process (as discussed in Sec. III D 6 for the case of quantum trajectories) also leads to a proper mixture. For example, this is well represented by open-system models of electron and exciton transport in disordered media [45].

Another important scenario where mixed states become necessary is that of composite systems, i.e., systems composed of two or more subsystems. As discussed in detail in Sec. II D, if the state of the total system is *entangled*, the state of a subsystem (i.e, the partial state) may need to be represented by a density operator, as shown in the example in script B.3 in Supplemental Material [33]. These mixed states are sometimes referred to as *improper mixtures* [43]. Improper mixtures become particularly important when one is studying entanglement of pure states that evolve unitarily. In such a case, purity and von Neumann entropy of partial states reveal how entangled a given subsystem is with respect to a given bipartition. However, this assessment becomes tricky for open systems, since their state becomes mixed also due to decoherence induced by the environment. Not surprisingly, much effort is being invested in finding faithfully and efficient measures of entanglement for mixed states [46–49].

C. Definition and properties of the density operator

Whether we are dealing with proper or improper mixtures of states, we can represent the set $\{|\psi_j\rangle, p_j\}$ using a linear operator on the Hilbert space,

$$\rho = \sum_{j=1}^{d} p_j |\psi_j\rangle\langle\psi_j|, \tag{7}$$

known as the density operator [41], where $|\psi_j\rangle\langle\psi_j|$ is the outer product of $|\psi_j\rangle$ with itself, that is, the vector product of $|\psi_j\rangle$ with its dual $\langle\psi_j|$. The coefficients $p_j > 0$ are such that $\sum_j p_j = 1$, since they represent probabilities (also known as *convex combination*). Density operators have three fundamental properties:

(1) *Hermitian*. $\rho = \rho^\dagger$. This implies that ρ has only real eigenvalues.
(2) *Positive* [50]. $\rho > 0$. That is, ρ eigenvalues $p_j \in [0, 1]$ are not negative.
(3) *Normalized*. $\mathrm{Tr}\rho = 1$, which can also be stated as $\sum_j p_j = 1$, i.e., the sum of its eigenvalues (probabilities) must add up to 1.

Density operators can represent both pure and mixed states, and can be expressed in any basis $\mathcal{B} = \{|\phi_i\rangle\}_{i=1}^{d}$ of the Hilbert space $\mathcal{H}$ as

$$\rho = \sum_{i,j=1}^{d} \rho_{ij} |\phi_i\rangle\langle\phi_j| = \begin{pmatrix} \rho_{11} & \rho_{12} & \cdots & \rho_{1d} \\ \rho_{21} & \rho_{22} & \cdots & \rho_{2d} \\ \vdots & \vdots & \ddots & \vdots \\ \rho_{d1} & \rho_{d2} & \cdots & \rho_{dd} \end{pmatrix}, \tag{8}$$

where ρ_{ij} is the associated matrix element with row i and column j. The diagonal elements ρ_{ii} of the density matrix are known as *populations* and they denote the probabilities of finding the system in the respective basis states $|\phi_i\rangle$. The off-diagonal elements ρ_{ij} are known as *coherences*, and provide information about the coherent superposition of the basis states $|\phi_i\rangle$ and $|\phi_j\rangle$ [51].

Similarly to state vectors, density operators encode all the available information that can be extracted from the considered system. For example, the expectation value of some observable $\mathcal{A}$ associated with Hermitian operator A can be calculated as

$$\langle A\rangle = \mathrm{Tr}[A\rho]. \tag{9}$$

The PYTHON script B.2 in Supplemental Material [33] provides an implementation of a density operator and the evaluation of the expectation value of some observable.

There we consider a system with dimension $d = 3$ in a mixed state defined by state vectors $\{|\psi_1\rangle, |\psi_2\rangle, |\psi_3\rangle\}$ with probabilities $\{0.1, 0.3, 0.6\}$ and represented by the density operator $\rho = 0.1|\psi_1\rangle\langle\psi_1| + 0.3|\psi_2\rangle\langle\psi_2| + 0.6|\psi_3\rangle\langle\psi_3|$.

D. Composite systems

Composite systems consist of two or more (interacting) quantum systems, whose Hilbert space is given by the tensor product of the individual Hilbert subspaces, $\mathcal{H} = \bigotimes_i \mathcal{H}_i$ [41]. For example, a composite system might be given by a pair of interacting two-level systems (*qubits*, in quantum information theory) or by a system S interacting with some large environment E.

1. Tensor product and partial trace

Any state ρ of a composite system can be represented with use of a basis $\mathcal{B}$ constructed with use of the *tensor product* of the basis elements of each subsystem's basis $\mathcal{B}_\alpha = \{|\phi_i\rangle_\alpha\}_{i=1}^{d_\alpha}$. For example, a bipartite system can be expressed in the following basis:

$$\mathcal{B} = \left\{|\phi_i\rangle_1 \otimes |\phi_j\rangle_2\right\}_{i,j}. \tag{10}$$

In PYTHON, the tensor product can be implemented with NUMPY with use of the Kronecker product `kron`:

```
psi = numpy.kron(psi1,psi2)
```

Similar implementations are available in MATHEMATICA and MATLAB, with `KroneckerProduct` and `kron`, respectively. Note that the matrix element ordering in the implementation of the Kronecker product is chosen by convention. As a result, the Kronecker product is implemented in slightly different ways across different programming languages [52].

By generalizing Eq. (10) to N-body systems, we can also write any N-body state using the local product basis as

$$|\psi\rangle = \sum_{\alpha_1,\ldots,\alpha_N} \psi_{\alpha_1,\ldots,\alpha_N} |\alpha_1\rangle_1 \otimes \cdots \otimes |\alpha_N\rangle_N, \tag{11}$$

$$= \sum_{\boldsymbol{\alpha}} \psi_{\boldsymbol{\alpha}} |\alpha_1 \cdots \alpha_N\rangle, \tag{12}$$

where $\boldsymbol{\alpha} = (\alpha_1, \ldots, \alpha_N)$, and $\{\alpha_i\}$ is a d_i-dimensional set of indices that spans all the local states of subsystem i. Equation (12) is a shorthand notation in which the tensor products are implicitly absorbed in the definition of the basis states. However, when one is handling many-body systems, it is essential to maintain the ordering chosen for the tensor product composition. This becomes particularly evident when one is defining and handling local operators, i.e., operators that act only on one subsystem, such as

$$A_i = \mathbb{1}_1 \otimes \cdots \otimes a_i \otimes \cdots \otimes \mathbb{1}_N, \tag{13}$$

where a_i is some operator on the local Hilbert space $\mathcal{H}_i$, while A_i is the operator as defined on the full N-body system. In other words, when constructing N-body states and operators, we must be consistent in the ordering of Kronecker products and the placement of identity operators.

When one is calculating expectation values of composite systems, it may be useful to focus only on the *marginal state* of one of the subsystems. The marginal state ρ_1 of subsystem $\alpha = 1$ is obtained from the total state ρ by one *tracing over* the degrees of freedom associated with the rest of the Hilbert space (here subsystem 2):

$$\rho_1 = \mathrm{Tr}_2[\rho]. \tag{14}$$

The linear operator $\mathrm{Tr}_\alpha[\cdot]$ is called the "partial trace," and its definition can be found in Ref. [26]. Note that calculation of the expectation value of local observables, i.e., acting only on a given subsystem i, requires knowledge of only the marginal $\rho_i = \mathrm{Tr}_{\bar{i}}[\rho]$, where here $\mathrm{Tr}_{\bar{i}}$ represents the partial trace over all the subsystems except for i. For the case of bipartite systems with dimensions d_1 and d_2, the partial trace can be implemented in PYTHON with use of NUMPY as follows:

```
rho1 = np.trace(rho.reshape(d1,d2,d1,d2),
                axis1=1, axis2=3)
rho2 = np.trace(rho.reshape(d1,d2,d1,d2),
                axis1=0, axis2=2)
```

In the code snippet above, the full density operator `rho` first represented as a $d_1 d_2 \times d_1 d_2$ matrix, is reshaped into a $d_1 \times d_2 \times d_1 \times d_2$ tensor. Then, the partial trace is evaluated by one choosing the subarrays whose trace needs to be returned. Following the ordering chosen with `kron`, to obtain ρ_1 we trace over the subarrays associated with subsystem 2, i.e., `axis1=1` and `axis2=3`.

For example, let us consider the following bipartite pure state:

$$|\psi(\theta)\rangle = \cos(\theta)|00\rangle + \sin(\theta)|11\rangle, \tag{15}$$

where $|00\rangle = |0\rangle_1 \otimes |0\rangle_2$, $|11\rangle = |1\rangle_1 \otimes |1\rangle_2$, and its associated density operator is given by $\rho(\theta) = |\psi(\theta)\rangle\langle\psi(\theta)|$. The state $\rho(\theta)$ is separable for $\theta = 0, \pi/2$, and is entangled otherwise, being maximally entangled [53] for $\theta = \pi/4$. As a result, for $\theta \neq k\pi/2$, the partial state of each subsystem $\rho_i(\theta) = \mathrm{Tr}_j[\rho(\theta)]$ is not pure, and is therefore an improper mixture. To measure the degree of mixedness of

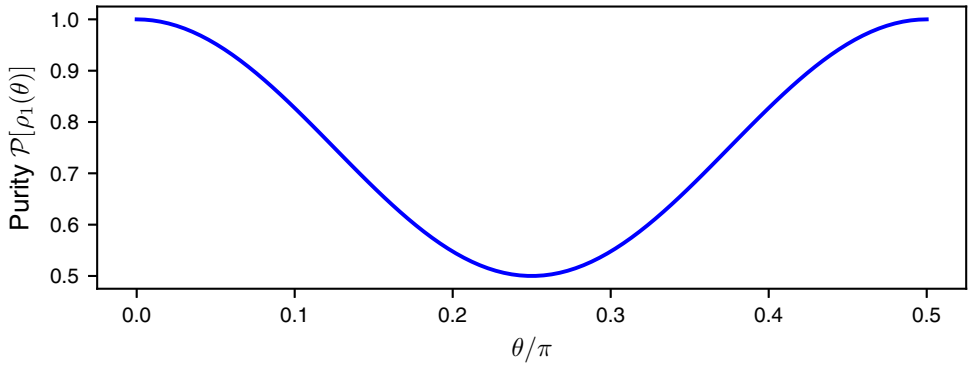

FIG. 2. Purity of the marginal state $\rho_1(\theta) = \mathrm{Tr}_2\rho(\theta)$, calculated using script B.3 in Supplemental Material [33] (see the script for parameter values). The state $\rho_1(\theta)$ is maximally mixed for $\theta = \pi/4$, since $\rho(\pi/4)$ is maximally entangled. This is an example of an improper mixture.

a density operator, we can use a figure of merit known as *purity* $\mathcal{P}$,

$$\mathcal{P}[\rho] = \mathrm{Tr}[\rho^2] = \sum_{j=1}^{d} p_j^2, \tag{16}$$

which is bounded between 1, for pure states $\rho = |\psi\rangle\langle\psi|$, and $1/d$, for maximally mixed states $\rho = \mathbb{1}/d$. The PYTHON script B.3 in Supplemental Material [33] calculates the marginal state of the first subsystem, $\rho_1(\theta) = \mathrm{Tr}_2\rho(\theta)$, showing that its purity $\mathcal{P}[\rho_1(\theta)] < 1$ for $\theta \neq k\pi/2$. Notice that $\rho_1(\theta)$ is maximally mixed when $\rho(\theta)$ is maximally entangled, i.e., $\mathrm{Tr}\rho_1(\pi/4) = 1/2$, as shown in Fig. 2.

A powerful implementation of the tensor product and the partial trace (`ptrace`) for any type of composite system is available in QUTIP, as shown in script C.1 in Supplemental Material [33]. See Refs. [34,41] for more on composite systems and Refs. [48,54,55] for an in-depth analysis of entanglement and other quantum correlations. For more on purity, entropy, measures of distinguishability, and other information-theoretic figures of merit, see Refs. [41,54].

2. Direct sum

Sometimes it is useful to compose systems given by the *addition* of different Hilbert spaces. For example, when one is studying a pair of interacting systems with Hilbert space $\mathcal{H}_a = \mathcal{H}_1 \otimes \mathcal{H}_2$ and dimension d_a, it might be convenient to add some states $\{|\phi_i\rangle_b\}_{i=1}^{d_b}$ to the picture, perhaps representing the result of some transitions that are modeled phenomenologically. In these cases the total Hilbert space is given by

$$\mathcal{H} = \mathcal{H}_a \oplus \mathcal{H}_b. \tag{17}$$

Explicitly, the direct sum between vectors $\mathbf{u} = (u_1, u_2)^T$ and $\mathbf{v} = (v_1, v_2, v_3)^T$ is conventionally given by $\mathbf{u} \oplus \mathbf{v} = (u_1, u_2, v_1, v_2, v_3)^T$. Numerically, a basis for this space can be constructed, from the bases of each individual subsystem, with use of a block matrix structure,

$$M = \begin{pmatrix} M_a & \mathbf{0} \\ \mathbf{0}^{\mathrm{T}} & M_b \end{pmatrix}, \tag{18}$$

where M_a and M_b are $d_a \times d_a$ and $d_b \times d_b$ matrices, respectively, and $\mathbf{0}$ is a $d_a \times d_b$ matrix. The above structure can be implemented in PYTHON as shown in script B.4. For more information on tensor products, direct sums, and irreducible representations, see Ref. [34].

E. Schrödinger and von Neumann equations

When one is studying the dynamics of quantum systems using the density operator representation, Schrödinger's equation (3) becomes

$$\dot{\rho}(t) = -\frac{i}{\hbar}[H, \rho(t)], \tag{19}$$

which is known as the *von Neumann equation* [56], where H is the Hamiltonian of the system (which can be time dependent), $\dot{\rho} = \partial_t\rho$, and $[\cdot,\cdot]$ is the commutator [26]. In general, the solution to this equation is given by some unitary operator $U(t; t_0)$ that propagates the state of the system from some initial time t_0 to some time t,

$$\rho(t) = U(t; t_0)\rho(t_0)U(t; t_0)^\dagger, \tag{20}$$

where $\dagger$ is the conjugate transpose (*adjoint*). If H is time independent, the solution is given by $U(t; t_0) = \exp[-iH(t - t_0)/\hbar]$ and can be reduced to $U(\tau) = \exp[-iH\tau/\hbar]$ for all t, t_0 such that $\tau = t - t_0$. See Ref. [26,57] for more on the solution U for the time-dependent Hamiltonian using time-ordering operators and the Dyson series.

1. Open quantum systems

The focus of this tutorial is the dynamics of systems that interact with their surrounding environment. These can be seen as being composed of a system of interest S and an environment E that is usually large, uncontrollable, or not experimentally accessible [26]. The dynamics of the full composite system S-E (or *universe*) follows Eq. (19) with Hamiltonian

$$H = H_S + H_E + H_{\text{int}}, \tag{21}$$

where H_{int} represents the interaction between the system with Hamiltonian H_S and the environment with Hamiltonian H_E.

If the solution $U(t;t_0)$ is known, the dynamics of the system S can be drawn from the state of the universe ρ by one tracing over the environment's degrees of freedom,

$$\rho_S(t) = \text{Tr}_E\big[\rho(t)\big]. \tag{22}$$

However, finding U for large composite systems is often a difficult problem, both numerically and analytically. Instead, we may seek to obtain a prescription for the dynamics of the system's state by performing the partial trace of Eq. (19), to obtain

$$\dot{\rho}_S(t) = -\frac{i}{\hbar}\text{Tr}_E\big\{[H,\rho(t)]\big\}. \tag{23}$$

Equation (23) provides the starting point for the derivation of density operator master equations such as those reviewed in Secs. III and IV.

III. DENSITY OPERATOR MASTER EQUATIONS

Density operator master equations are a powerful tool to study the dynamics of quantum systems that interact weakly [58] with their surrounding environment. Originally developed in the field of quantum optics to study light-matter interactions [1], they are also used to interpret the effect of noise in quantum information processing [41], transient emission and absorption spectra of optically active materials [59], and electronic and nuclear spin resonance experiments [60].

The power of master equations resides in the choice of ignoring the environment's dynamics, which is often uncontrollable and inaccessible. By ignoring the environment's degrees of freedom, we can limit the scaling of the computational requirements to a polynomial of $d = \dim\mathcal{H}_S$, where $\mathcal{H}_S$ is the system's Hilbert space. In this section we introduce quantum master equations and focus on their numerical implementation and solution, providing direction for further reading.

A. Introduction to the Lindblad master equation

The paradigmatic example of a density operator master equation is the Gorini-Kossakowski-Sudarshan-Lindblad (GKSL) master equation [61–64], often known as the *Lindblad master equation*,

$$\dot{\rho}(t) = -\frac{i}{\hbar}[H,\rho(t)] + \sum_k \gamma_k\left[L_k\rho(t)L_k^\dagger - \frac{1}{2}\left\{L_k^\dagger L_k,\rho(t)\right\}\right], \tag{24}$$

where ρ is the system's density operator [65], H is the Hamiltonian of the system [66], and $\{L_k\}$ are the Lindblad operators [67] representing some nonunitary processes such as relaxation or decoherence that occur at some rates $\{\gamma_k\}$. The operators $[.,.]$ and $\{.,.\}$ denote the commutator and anticommutator of the operands. From now on, H represents the Hamiltonian of the system, unless specified otherwise.

Like the Hamiltonian generates coherent dynamics, the Lindblad operators [68] generate incoherent transitions in the space of states. Unlike the Hamiltonian, they do not need to be Hermitian. For example, a decay transition from some excited state $|e\rangle$ to some ground state $|g\rangle$ is mediated by the Lindblad operator

$$L_\downarrow = |g\rangle\langle e|. \tag{25}$$

Indeed, when we apply $L_\downarrow$ to $|e\rangle$, we obtain $|g\rangle = L_\downarrow|e\rangle$. Note that $L_\downarrow^\dagger = |e\rangle\langle g| \neq L_\downarrow$.

Equation (24) is used to approximate the evolution of the density operator of a system S with Hamiltonian H that is weakly coupled to a *Markovian* (memoryless stochastic process) environment [26]. The GKSL master equation is the general form for a completely positive and trace-preserving Markovian and time-homogeneous map for the evolution of the system's density operator ρ [26]. A discussion of the motivations for these requirements can be found in Refs. [26,64]. Derivations of Eq. (24) can be found in Refs. [26,51,69].

1. Microscopically derived and phenomenological Lindblad master equation

Before looking at the solution of the GKSL master equation, we briefly discuss its motivation from a mathematical and microscopic perspective. As anticipated in Sec. II E 1, quantum master equations are rigorously obtained from a microscopic description of the system and the environment, i.e., prescribed by a system-environment Hamiltonian H_{tot} such as

$$H_{\text{tot}} = H + \sum_\alpha A_\alpha \otimes B_\alpha + H_E, \tag{26}$$

with H (H_E) being the system (environment) Hamiltonian and $\{A_\alpha\}$ ($\{B_\alpha\}$) being a set of system (environment)

coupling operators. As we discuss further in Sec. IV, the *microscopic derivation* of Eq. (24) proceeds via a sequence of approximations (Born, Markov, and secular), under the assumption that the system-environment couplings are weak when compared with the other characteristic energies. These approximations guarantee that Eq. (24) propagates any system's density operator into a well-defined state for all times. A microscopic derivation is also essential to reveal the nature and timescales of the decoherence and relaxation channels that affect the system, meaning that Lindblad operators $\{L_k\}$ and rates γ_k are obtained directly from the system spectrum, the coupling operators A_α, the environment's state ρ_E, and its correlation functions $\langle B_\alpha(\tau)B_\beta(0)\rangle$. The interested reader can find a detailed derivation of the GKSL master equation and its approximation in Refs. [26,69].

When a microscopic model of the system-environment interactions is not available, for example, due to inaccessibility of some of the environmental microscopic degrees of freedom, one can obtain a *phenomenological* quantum master equation, starting from evident (and potentially experimentally accessible) incoherent processes that affect the system. To obtain a master equation from phenomenological arguments, one can construct the Lindblad operators $\{L_k = |\psi_k\rangle\langle\psi'_k|\}$ associated with the transitions $|\psi'_k\rangle \to |\psi_k\rangle$, which happen at some rate γ_k, where $|\psi_k\rangle$ are some states of the system.

Here we stress the fact that, when possible, a microscopic derivation is always preferable to a phenomenological one. The latter is more suitable for toy models and may result in an inexact description of decoherence channels and rates. In this tutorial, we discuss examples of using either approach. For simplicity, we begin from phenomenological master equations, proceeding to the microscopic derivations of Lindblad and Bloch-Redfield master equations in Sec. IV.

B. The Liouville superoperator

When one is solving Eq. (24), it is convenient to express the master equation in a vector notation,

$$\dot{\boldsymbol{\rho}} = \mathcal{L}\boldsymbol{\rho}, \tag{27}$$

known as *superoperator* or *Liouville* form, where $\boldsymbol{\rho} = \mathrm{vec}(\rho)$ is the *vectorized* form of ρ and $\mathcal{L}$ is the superoperator associated with the generator $\dot{\rho}$ of Eq. (24). The matrix associated with the density operator ρ can be reshaped into a vector in many equivalent ways [70], resulting in different superoperators. Any reshaping is valid, as long as one keeps track of the ordering in the elements of the superoperator. Script B.5 in Supplemental Material [33] illustrates reshaping via the NUMPY method `reshape`. Similar methods are available in MATHEMATICA and MATLAB.

To see how the representation of Eq. (27) comes about, it is instructive to first write Eq. (24) in terms of the matrix elements of the density operator $\dot{\rho}_{ij} = \mathcal{L}_{ij,kl}\rho_{kl}$, where the sum over kl is omitted with use of Einstein's notation. From this notation it is clear that the Liouville superoperator in this form is a four-legged tensor (i.e., it has four indices). Then one can merge pairs of indices as $\alpha = f(i,j)$ and $\beta = f(k,l)$ to obtain $\dot{\rho}_\alpha = \mathcal{L}_{\alpha,\beta}\rho_\beta$, thus effectively obtaining Eq. (27). Since the choice of reshaping function f is arbitrary, one must be consistent when performing this operation. Alternatively, one can work directly with the tensor representation of the superoperator $\mathcal{L}_{ij,kl}$, which can help in reducing the computational cost of solving the dynamics (e.g., when one is using finite-difference methods). From this tensor notation it is possible to entirely forego the reshaping, and use numerical methods such as NUMPY's `einsum`, which perform Einstein summation according to a chosen convention. However, it is important to keep in mind that some numerical solvers (such as `odeint` in SCIPY) support working only with vectors, and thus reshaping often becomes a necessity.

A robust implementation of the reshaping is implemented in QUTIP with the methods `operator_to_vector` and `vector_to_operator`. Nevertheless, it is important to keep in mind that one must be careful when one is reshaping superoperators into operators (and vice versa), again due to the ordering conventions of different Kronecker product implementations.

1. Constructing the Liouville superoperator

While the superoperator $\mathcal{L}$ can be constructed "by hand" for small systems, it is advisable to have a systematic approach to compile it from some Hamiltonian H and some Lindblad operators $\{L_k\}$. Two common ways are to either follow an index prescription for the superoperator tensor $\rho_{ab} = \sum_{cd}\mathcal{L}_{abcd}\rho_{cd}$ or to use the following linear algebra identity for the column-ordered form of $\mathrm{vec}(\rho)$ [71,72]:

$$\mathrm{vec}(AXB) = (B^{\mathrm{T}} \otimes A)\mathrm{vec}(X). \tag{28}$$

To take advantage of the latter, we proceed by inserting the identity operator $\mathbb{1}$ into Eq. (24),

$$\mathbb{1}\dot{\rho}\mathbb{1} = -\frac{i}{\hbar}\Big(H\rho\mathbb{1} - \mathbb{1}\rho H\Big) + \sum_k \gamma_k\left[L_k\rho L_k^\dagger - \frac{1}{2}\Big(L_k^\dagger L_k\rho\mathbb{1} + \mathbb{1}\rho L_k^\dagger L_k\Big)\right], \tag{29}$$

from which the superoperator can be easily constructed with use of the tensor product structure discussed in Sec. II D and implemented with the `kron` method in PYTHON and MATLAB or the `KroneckerProduct` function in MATHEMATICA. Combining Eqs. (27)–(29), we

obtain

$$\mathcal{L} = -\frac{i}{\hbar}\Big(\mathbb{1}\otimes H - H^{\mathrm{T}}\otimes\mathbb{1}\Big) + \sum_k \gamma_k\Big[L_k^*\otimes L_k - \frac{1}{2}\Big(\mathbb{1}\otimes L_k^\dagger L_k + L_k^{\mathrm{T}}L_k^*\otimes\mathbb{1}\Big)\Big]. \tag{30}$$

The PYTHON script B.6 in Supplemental Material [33] implements Eq. (30) using NUMPY arrays. It is worth noting that here the rates γ_k are embedded into the Lindblad operators via $L_k \to L_k' = \sqrt{\gamma_k}L_k$ for a simpler implementation. As discussed in the next sections, the superoperator form offers a direct pathway to solving Eq. (24) based on the solution of a system of linear ordinary differential equations.

Before we proceed, let us discuss the operation and memory cost associated with constructing the superoperator. By reshaping the Hamiltonian and jump operators, we go from a $d \times d$ to a $d^2 \times d^2$ dense matrix representation for a single-body system with dimension d. For an N-body system with local dimension d, a dense superoperator representation grows exponentially as $d^{2N} \times d^{2N}$. Fortunately, for most physical systems the Liouvillian is sparse and therefore the operations and memory cost associated with its construction can be afforded even for some classes of many-body systems (see Refs. [73,74] for an introduction to tensor network methods for many-body quantum systems and ITensor for some efficient implementation using the languages C++ and JULIA). Arguably, except for small systems, one should always aim to construct a sparse superoperator. Furthermore, some time-evolution and steady-state solution algorithms (e.g., finite-difference methods) do not need the full Liouvillain $\mathcal{L}$ but rather need the function $\mathcal{F} : \rho \to \dot{\rho}$, which can be easily constructed directly from Eq. (24) (an example of this function can be found in the PYTHON script B.15 in Supplemental Material [33]). The computational cost of evaluating this function is, in general, lower than that required to construct the full Liouvillian, since it is evaluated for a specific state from a usually small set of operators (H and L_k) that also tend to be sparse.

C. Steady-state solution

Before we look at the dynamics $\rho(t)$ of the density operator, let us discuss some methods to obtain the steady-state solution of Eqs. (24) and (27).

1. Use of the null space of the Liouville superoperator

Once we have expressed a linear master equation in the superoperator form, we can use the matrix $\mathcal{L}$ to study the behavior of the system. Of immediate interest is the steady-state solution ($\dot{\rho} = 0$), which is often measured directly in experiments. To find any steady-state solutions, we solve for the *null space* of $\mathcal{L}$ [75], which is the subspace of all vectors $\boldsymbol{\rho}$ that satisfy the equation

$$\mathcal{L}\boldsymbol{\rho} = 0. \tag{31}$$

Numerically, this can be done with use of the `NullSpace` function in MATHEMATICA, the `null` function in MATLAB, or the `null_space` method in the NUMPY library SCIPY. An analytic solution can also be sought with this approach with MATHEMATICA or with SYMPY in PYTHON.

If there is a unique solution, solving for the null space will provide the corresponding steady-state density matrix vector $\boldsymbol{\rho}(\infty)$ up to a constant factor, the value of which is given by the original normalization condition $\mathrm{Tr}(\rho) = 1$. If there are multiple solutions, solving for the null space will give linearly independent vectors. In such a case, the steady state depends on the initial state of the system. For example, let us consider a two-level system Hamiltonian [76] H with energy splitting Δ and coupling Ω, and Lindblad operators $L_\downarrow$ and L_0 associated with spontaneous relaxation (loss of energy) and dephasing (decay of coherences), respectively,

$$H = \hbar\begin{pmatrix} 0 & \Omega \\ \Omega & \Delta \end{pmatrix}, \tag{32}$$

$$L_\downarrow = \sqrt{\gamma_\downarrow}\begin{pmatrix} 0 & 1 \\ 0 & 0 \end{pmatrix}, \tag{33}$$

$$L_0 = \sqrt{\gamma_0}\begin{pmatrix} 0 & 0 \\ 0 & 1 \end{pmatrix}, \tag{34}$$

where $\gamma_\downarrow$ and γ_0 are the rates associated with relaxation and dephasing. In the PYTHON script B.7 in Supplemental Material [33], we construct $\mathcal{L}$ in PYTHON and solve for its null space for the case of (1) driving and relaxation with no dephasing, $\gamma_0 = 0$, and (2) dephasing and no driving or relaxation, $\Omega, \gamma_\downarrow = 0$. In case (1), there is a unique steady state that becomes $\boldsymbol{\rho}(\infty) = (1,0,0,0)^{\mathrm{T}}$ for $\Omega = 0$, i.e., the ground state of the system, as expected for a two-state system undergoing spontaneous relaxation with no driving field. Instead, for the case of dephasing and no driving, the `null` function returns two vectors $\boldsymbol{\rho}(\infty) = (1,0,0,0)^{\mathrm{T}}, (0,0,0,1)^{\mathrm{T}}$, i.e., the ground and excited states. Their convex hull is a one-dimensional linear subspace associated with all possible steady states of $\mathcal{L}$. In this case, the specific steady state depends on the choice of initial state. See Sec. C in Supplemental Material [33] for a MATLAB implementation of the method used in script B.7.

2. Iterative methods

Most of the available null space solvers, such as `scipy.null_space`, are based on the use of the singular value decomposition. For this reason, their computational cost scales rapidly with the size of the system,

making them rather ineffective beyond small systems and toy models. A common strategy to tackle large problems consists in using iterative solvers [77], such as SCIPY's `bicg`, `bicgstab`, `gmres`, and `minres`. These are often used in conjunction with an efficient approach to calculate $\dot{\rho}$ (such as the one based on sparse arrays given in script B.5 in Supplemental Material [33]) together with a renormalization constraint. These methods can be scaled up to exceptionally large systems thanks to their numerical efficiency and, if there is a single solution, they are guaranteed to converge.

3. Algebraic solution

The steady state solution $\rho(\infty)$ for both linear and nonlinear [78] generators can be obtained by our solving Eq. (24) for $\dot{\rho} = 0$ algebraically or symbolically. Solving a system of symbolic equations becomes rapidly very expensive and therefore it is often only feasible for small systems. When possible, however, symbolic solutions provide insightful analytic expressions that are easy to interpret. In PYTHON, algebraic solutions can be sought with use of the `solve` method of the SYMPY library, as demonstrated in script B.8 in Supplemental Material [33] for the case of $\Omega = 0$, $\gamma_0 = 0$, with respect to Eq. (32).

Algebraic solutions can also be sought in MATLAB with `solve` or in MATHEMATICA with use of the `Solve` method. These provide a more straightforward approach to solving symbolic matrix equations. A MATLAB implementation of script B.8 can be found Supplemental Material [33] in script C.2.

D. Solving the dynamics of the system

We now discuss how to solve Eq. (24) in order to obtain the state of the system $\rho(t)$ at any time t from a given initial condition $\rho_0 = \rho(t_0)$. Let us represent the solution with the dynamical map $\rho(t) = \Lambda(t; t_0)[\rho_0]$. For linear, time-independent generators $\mathcal{L}$, the solution to Eq. (27) can be obtained by our calculating the following matrix exponential [26]:

$$\boldsymbol{\rho}(t) = \exp\left[\mathcal{L}(t - t_0)\right]\boldsymbol{\rho}(t_0). \tag{35}$$

The operator $P(t; t_0) = \exp\left[\mathcal{L}(t - t_0)\right]$ is called the "propagator" of the evolution. In Eq. (35) we have implicitly represented the propagator $P(t; t_0)$ as a matrix, i.e., by our applying the same reshaping function that we used to vectorize $\rho \to \boldsymbol{\rho}$ to both of its index pairs. Then one can represent the solution as a density operator $\rho(t)$ just by applying the inverse reshaping on $\boldsymbol{\rho}(t)$. The propagator can also be stored as a four-legged tensor $P_{ij,kl}(t; t_0)$, in which case the solution reads $\rho_{ij}(t) = P_{ij,kl}(t; t_0)\rho_{kl}(t_0)$. See Ref. [69] for details on how to obtain the dynamical map Λ from P using, for example, a Kraus operator representation. Equation (35) is implemented in PYTHON with use of SCIPY in script B.9 in Supplemental Material [33], with the result shown in Fig. 3.

See script C.8 in Supplemental Material [33] for an implementation of Eq. (35) using MATLAB. Calculating the matrix exponential is just one of the many ways to solve the dynamics of the systems. In this section we touch upon several other approaches, some of which are briefly summarized in Table I.

Script B.10 in Supplemental Material [33] shows how to use Eq. (35) to study the effect of temperature on a physical implementation of a quantum logic gate [79]. In that example, we consider the Hadamard–controlled NOT (CNOT) gate [79], given by the sequential composition of the Hadamard gate H on the first qubit

$$U_1 = H \otimes \mathbb{1} := \frac{1}{\sqrt{2}}\begin{pmatrix} 1 & 1 \\ 1 & -1 \end{pmatrix} \otimes \mathbb{1}, \tag{36}$$

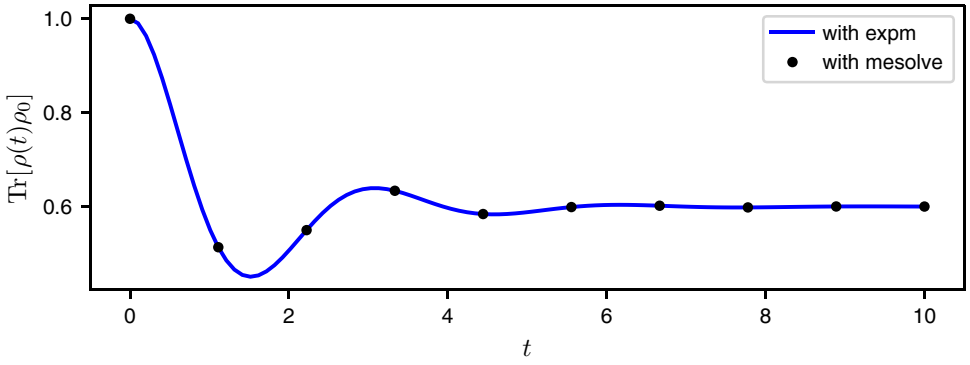

FIG. 3. Propagation using matrix exponential (`expm` from NUMPY), obtained with use of script B.9 in Supplemental Material [33]. The propagated state $\rho(t)$ is obtained with use of Eq. (35), and is compared with the solution obtained with use of a finite-difference method (`mesolve` from QUTIP) implemented in script C.5 in Supplemental Material [33] (see the script for parameter values).

TABLE I. Summary of the pros and cons of some methods to solve the dynamics of a single-body system with dimension d and dense representation. Refer to each section for more information on when to use each method and to Sec. III D 8 for sparse representations.

Method	Pros	Cons
Matrix exponential (Sec. III D)	Exact, reusable for different ρ_0.	$\mathcal{O}(d^4)$ memory and operations cost.
Action of matrix exponential (Sec. III D 8)	Exact, $\mathcal{O}(d^2)$ operations cost.	Not reusable for different ρ_0.
Diagonalization (Sec. III D 1)	Exact, reusable for different ρ_0.	Does not always exist.
Finite difference (Sec. III D 5)	$\mathcal{O}(d^2)$ memory and operations cost.	Approximate, not reusable for different ρ_0.
Quantum trajectories (Sec. III D 6)	$\mathcal{O}(d)$ memory cost, efficient disorder sampling.	Approximate.

and the CNOT gate

$$U_2 = \text{CNOT} := \begin{pmatrix} 1 & 0 & 0 & 0 \\ 0 & 1 & 0 & 0 \\ 0 & 0 & 0 & 1 \\ 0 & 0 & 1 & 0 \end{pmatrix}. \tag{37}$$

The resulting gate, shown in Fig. 4, can be used to obtain the (maximally entangled) Bell state

$$|\Phi_+\rangle = \frac{|00\rangle + |11\rangle}{\sqrt{2}} = U_2 U_1 |00\rangle, \tag{38}$$

starting from the fiducial input state $|00\rangle$. In practice, the gate is implemented by means of two time-independent Hamiltonians H_1 and H_2,

$$H_1 = \frac{1}{2}\left(\mathbb{1} - \frac{\sigma_z + \sigma_x}{\sqrt{2}}\right) \otimes \mathbb{1}, \tag{39}$$

$$H_2 = \frac{\mathbb{1} - \sigma_z}{2} \otimes \frac{\mathbb{1} - \sigma_x}{2}, \tag{40}$$

that act on some initial state for some time $\tau = \pi$ [80]. If the unitary gates U_j are also Hermitian, their generating Hamiltonians H_j can be obtained by diagonalization of the gates,

$$U_j = \sum_{k=0}^{\dim} \omega_k^{(j)} |\omega_k^{(j)}\rangle\langle\omega_k^{(j)}|, \tag{41}$$

to obtain $U_j = \exp[-i\pi H_j]$, with $H_j = |\omega_0^{(j)}\rangle\langle\omega_0^{(j)}|$.

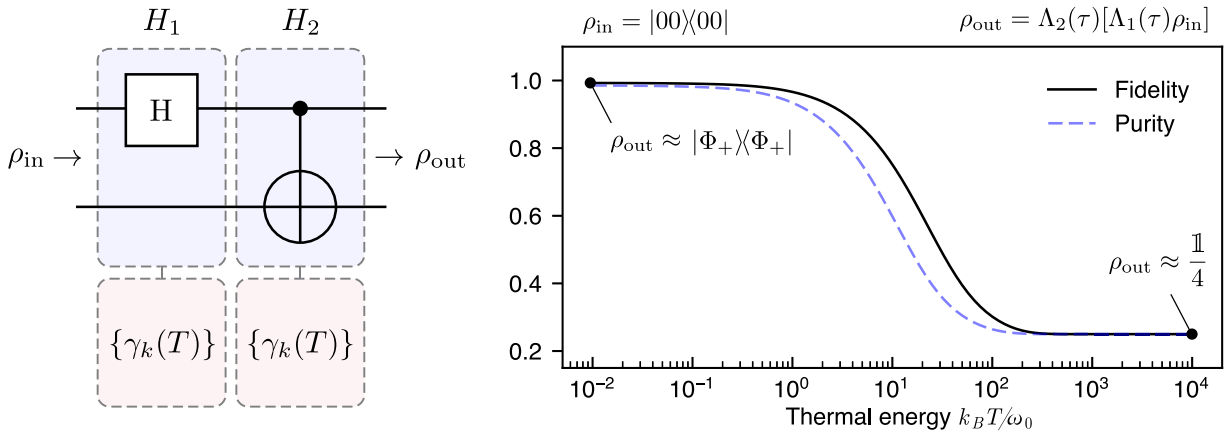

FIG. 4. Left: A Hadamard-CNOT gate is implemented with two time-independent Hamiltonians H_1 and H_2. A temperature-dependent decoherence process affects the performance of the gate implementation via dephasing and relaxation rates $\{\gamma_k(T)\}$, which are greater as the thermal energy $k_B T$ increases with respect to the energy gap $\hbar\omega_0$ between ground $|0\rangle$ and excited $|1\rangle$ states, with k_B being the Boltzmann constant. As a result, the output state $\rho_{\text{out}} = \Lambda_2(\tau)[\Lambda_1(\tau)[\rho_{\text{in}}]]$ differs from the target state $|\Phi_+\rangle = U_2 U_1 |00\rangle$, given in Eq. (38). Right: This difference is measured here with use of the fidelity $\mathcal{F}(\rho,\sigma) = (\text{Tr}[\sqrt{\sqrt{\rho}\sigma\sqrt{\rho}}])^2$, which is equal to 1 when $\rho = \sigma$, i.e., when $\rho_{\text{out}} = |\Phi_+\rangle\langle\Phi_+|$. For low temperature $k_B T \ll \omega_0$, the circuit well approximates the desired gate, while for high temperature $k_B T \gg \omega_0$, the information about the input states is completely lost due to decoherence, with $\rho_{\text{out}} = \mathbb{1}/4$ being the maximally mixed state. The purity of the output state $\mathcal{P}[\rho_{\text{out}}] = \text{Tr}[\rho_{\text{out}}^2]$ shows that as the temperature increases, the implemented gate is no longer unitary, and instead maps an initially pure state to a mixed state. This figure is obtained using script B.10 in Supplemental Material [33] (see the script for parameter values).

In practice, decoherence processes, such as dephasing and relaxation, prevent us from implementing ideal unitary gates as U_1 and U_2. As a result, the output state is, in general, a mixed state, $\rho_{\text{out}} = \Lambda_2(\tau)[\Lambda_1(\tau)[\rho_0]]$. In this example, the effect of temperature is modeled via some temperature-dependent transition rates $\gamma_k(T)$, which are greater as the temperature increases, as prescribed by Bloch-Redfield theory, as discussed in Sec. IV.

It is worth pointing out that the approach used in script B.9 is by no means optimized, and calculates a new propagator for every time step in the time domain considered. When working with evenly spaced time steps, we can reduce the computational cost by using the composition rule of dynamical semigroups, as discussed in Sec. III D 2. In QUTIP, instead, the solution is obtained with use of the `mesolve` method, which by default uses SCIPY's numerical integration library `integrate`.

1. Decomposition of the Liouville superoperator

The superoperator $\mathcal{L}$ is generally a complex, non-Hermitian matrix. For this reason a spectral decomposition of $\mathcal{L}$ is not always guaranteed [81]; that is, $\mathcal{L}$ may not admit the diagonal representation $\mathcal{L} = VDV^{-1}$, although it always admits a singular value decomposition [82] of the form $\mathcal{L} = U\Sigma V^\dagger$, where U and V are unitaries and Σ_{ii} are the singular values (real and non-negative).

Let us here assume that $\mathcal{L}$ can be diagonalized. Since it is not Hermitian [83], its eigenvalues λ_k will, in general, be complex. Furthermore, its left and right eigenvectors, which abide by the relationships [84]

$$\mathcal{L}\mathbf{R}_k = \lambda_k \mathbf{R}_k, \tag{42}$$

$$\mathbf{L}_k^\dagger \mathcal{L} = \lambda_k \mathbf{L}_k^\dagger, \tag{43}$$

do not need to coincide. Notice that both $\mathbf{R}_k$ and $\mathbf{L}_k$ are column vectors; hence, $\mathbf{L}_k^\dagger$ is a row vector. Each left and right eigenvector can be normalized via

$$\hat{\mathbf{R}}_k = \mathbf{R}_k \Big/ \sqrt{\mathbf{L}_k^\dagger \mathbf{R}_k}, \tag{44}$$

$$\hat{\mathbf{L}}_k^\dagger = \mathbf{L}_k^\dagger \Big/ \sqrt{\mathbf{L}_k^\dagger \mathbf{R}_k}. \tag{45}$$

The normalized eigenvector pairs then follow the usual orthonormalization condition [84],

$$\hat{\mathbf{L}}_i^\dagger \hat{\mathbf{R}}_j = \delta_{ij}. \tag{46}$$

The solution of Eq. (27) for a system with time-independent Liouville superoperator $\mathcal{L}$ can now be expressed as follows:

$$\boldsymbol{\rho}(t) = \sum_{k=1}^{d^2} \hat{\mathbf{L}}_k^\dagger \boldsymbol{\rho}(t_0) \hat{\mathbf{R}}_k e^{\lambda_k (t-t_0)}, \tag{47}$$

where d is the dimension of the Hilbert space. For an in-depth analysis of the information contained in the spectrum of the Liouvillian, see Ref. [85].

The advantage of expressing the time evolution in the form of Eqs. (35) and (47) is that it is exact (when the eigenvalues are found exactly) for all times and therefore does not depend on the step size or other operational details of the integration routine used to solve the differential equation. In the PYTHON script B.11 in Supplemental Material [33], we use SCIPY to obtain the temporal solutions for a system with

$$H = \hbar \begin{pmatrix} 0 & \Omega \\ \Omega & 0 \end{pmatrix}, \tag{48}$$

$$L = \begin{pmatrix} 0 & 1 \\ 1 & 0 \end{pmatrix}, \tag{49}$$

$$\boldsymbol{\rho}(0) = \big(0, 0, 0, 1\big)^{\mathrm{T}}, \tag{50}$$

using the spectral decomposition of $\mathcal{L}$. The solution is shown in Fig. 5. A MATLAB implementation of this method can be found in script C.6 in Supplemental Material [33].

2. Propagation via semigroup composition

The dynamical maps generated by a linear Markovian quantum master equation such as Eq. (24) are a family of single-parameter maps Λ_t that have the following composition property:

$$\Lambda_s \circ \Lambda_t = \Lambda_{s+t}, \quad t, s \geq 0. \tag{51}$$

They are therefore known as a *quantum dynamical semigroup*. Equation (51) can also be expressed as $\Lambda_s[\Lambda_t[\rho]] = \Lambda_{s+t}[\rho]$. For more on quantum dynamical semigroups, see Ref. [26]. Equation (51) can be expressed in the superoperator form as

$$P(s)P(t) = P(s+t), \quad t, s \geq 0, \tag{52}$$

which follows directly from the properties of the exponential and the fact that $[\mathcal{L}s, \mathcal{L}t] = 0$. Note that the above does not generally hold for time-dependent $\mathcal{L}(t)$ and nonlinear generators $\mathcal{L}(\rho(t))$.

When propagating a system in time over an evenly spaced time set $\{k\delta t\}_{k=1}^m$, we can use the composition rule of dynamical semigroups to vastly reduce the computational cost of propagation. Instead of calculating a new propagator $P(t_k)$ for each time step $t_k = t_0 + k\delta t$, we can

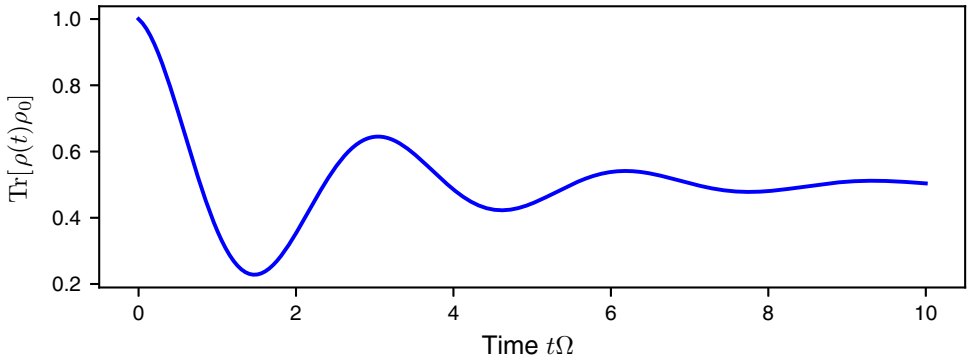

FIG. 5. Dynamics of the state $\rho(t)$ for Eq. (48), solving the Lindblad master equation with use of the normalized superoperator singular vectors, obtained with script B.11 in Supplemental Material [33] (see the script for parameter values).

calculate a single propagator $P_1 = P(\delta t)$ and obtain all the others using

$$P(t_k) = \prod_{j=1}^{k} P_1 = P_1^k. \tag{53}$$

The PYTHON script B.12 in Supplemental Material [33] implements Eq. (53); the results are shown in Fig. 6.

This approach is particularly useful when propagation is done for very long times or when large time steps are used, in which cases SCIPY's `integrate` methods usually tend to accumulate large numerical errors. For propagation over several orders of magnitude, it may be convenient to break each timescale into evenly spaced time steps to resolve the details of different dynamical transients. For example, this is useful when one is looking at dynamics from the femtosecond to nanosecond timescales.

3. Baker-Campbell-Hausdorff and Zassenhaus formula

Hamiltonians and superoperators are often sums of two or more terms, such as $W = U + V$. As briefly noted in Sec. III D 2, when the terms commute with each other $[U, V] = 0$, the solution can be obtained from the composition of individual terms. For example, let $\mathcal{L} = \mathcal{L}_1 + \mathcal{L}_2$, with $[\mathcal{L}_1, \mathcal{L}_2] = 0$. Then

$$P(t) = \exp(\mathcal{L}t) = \exp(\mathcal{L}_1 t)\exp(\mathcal{L}_2 t). \tag{54}$$

Instead, when considering pairs of noncommuting operators $[X, Y] \neq 0$, we have $\exp(X + Y) \neq \exp(X)\exp(Y) = \exp(Z)$. The solution to the latter equation for Z is known as the Baker-Campbell-Hausdorff formula [86] and reads

$$Z = X + Y + \frac{1}{2}[X, Y] + \frac{1}{12}\Big([X,[X,Y]] + [Y,[Y,X]]\Big) + \cdots. \tag{55}$$

The Baker-Campbell-Hausdorff solution finds application when used in the Zassenhaus formula, which allows us to decompose a matrix exponential $\exp[(X + Y)t]$, where t is

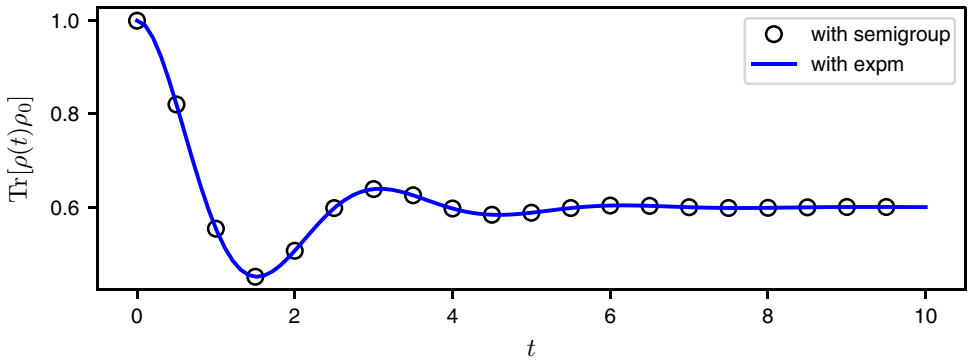

FIG. 6. Propagation using semigroup decomposition, obtained with script B.12 in Supplemental Material [33] (see the script for parameter values) compared with that obtained by computation of a new propagator for each time step.

a scalar parameter, in terms of a product series,

$$\exp[(X+Y)t] = \exp[Xt]\exp[Yt]\exp\left[-\frac{1}{2}[X,Y]t^2\right] \times \exp\left[\frac{1}{3}\left([Y,[X,Y]]+\frac{1}{2}[X,[X,Y]]\right)t^3\right]\cdots. \tag{56}$$

The formula is useful when the product series can be truncated or approximated to a certain set of terms. This is, for example, particularly useful when the generator is time-dependent $\mathcal{L}_t$ and $[\mathcal{L}_t, \mathcal{L}_s] \neq 0$: by choosing a sufficiently small time step δt such that $s = t + \delta t$, one can truncate the series in Eq. (56) to terms in $\mathcal{O}(\delta t^m)$ for some $m > 1$, as discussed in the next section.

4. Suzuki-Trotter expansion

A consequence of the Zassenhaus formula is that, for *small* time steps δt, Eq. (56) can be truncated to the first order in δt with errors on the order of $O(\delta t^2)$,

$$\exp[(X+Y)\delta t] = \exp[X\delta t]\exp[Y\delta t] + O(\delta t^2). \tag{57}$$

This can be used to obtain the solution for long times with use of the product series,

$$e^{(X+Y)t} = \lim_{n\to\infty}\left[\exp\left(X\frac{t}{n}\right)\exp\left(Y\frac{t}{n}\right)\right]^n, \tag{58}$$

also known as the *Suzuki-Trotter expansion* or the *Lie product formula* [86]. This approach is particularly useful when one is studying the dynamics of interacting many-body systems or time-dependent generators. The PYTHON script B.13 in Supplemental Material [33] uses the Suzuki-Trotter expansion to propagate a system by separating the contribution of the two noncommuting superoperators. The results are shown in Fig. 7.

5. Numerical solution with finite-difference methods

While the matrix exponential is a powerful tool to obtain the exact solution of Eq. (27), it may be less computationally expensive to compromise some precision in favor of less demanding time and memory requirements. Not only can finite-difference methods be efficient in solving density operator master equations, they can also be used to solve the dynamics of nonlinear and time-dependent generators. In this case, the approach consists in solving the set of coupled differential equations obtained by element-wise comparison of the left-hand and right-hand sides of Eq. (24).

Script B.14 in Supplemental Material [33] is a continuation of script B.11 and solves the dynamics of the same two-level system using the fourth-fifth order Runge-Kutta differential equation method. The method is implemented with use of the initial-value problem solver `solve_ivp` from the `scipy.integrate` library for PYTHON. The solution is shown in Fig. 8. A MATLAB implementation of the same code can be found in script C.8 in Supplemental Material [33].

6. Solution using the stochastic wave function method

Since the number of complex floating-point numbers required to represent superoperators such as $\mathcal{L}$ and P scales as d^4, memory may become an issue for large systems [87]. To circumvent this problem, we can propagate a density operator using the stochastic wave function method [1], also known as the *Monte Carlo wave function method* or *master equation unraveling*. Originally developed for quantum optics, the method is an adaptation of the kinetic Monte Carlo method [88] to the solution of Eq. (24). This approach can also be used to efficiently average over disorder realizations by resampling the disorder at each trajectory [89,90].

Instead of propagating a density operator solving Eq. (27), the method provides a procedure to propagate a state vector $|\psi_0\rangle$ under the influence of some generator $\mathcal{L}$

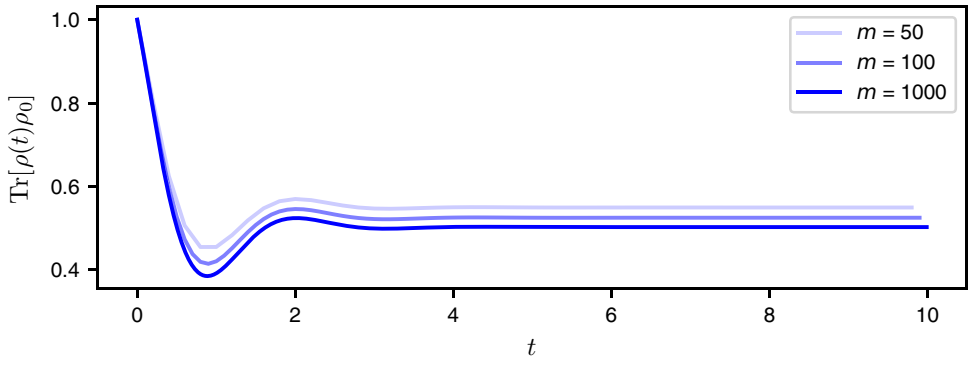

FIG. 7. Propagation using Suzuki-Trotter expansion for different numbers m of time steps (50, 100, and 1000) obtained with script B.13 in Supplemental Material [33] (see the script for parameter values).

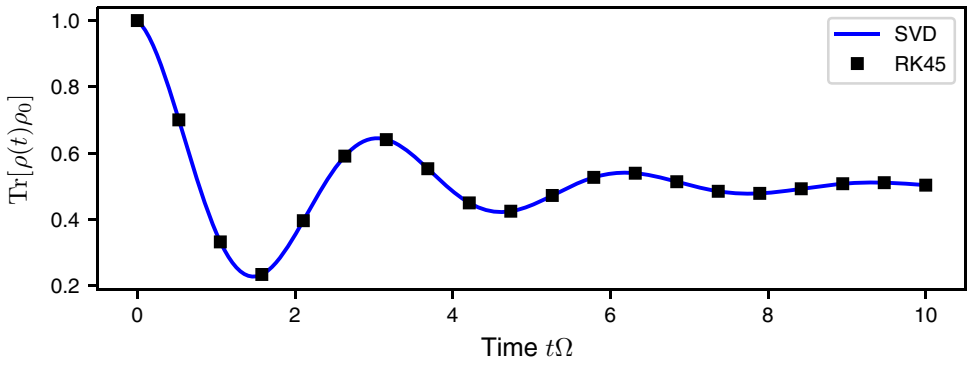

FIG. 8. Propagation using the finite-difference approach, based on the fourth-fifth order Runge-Kutta method (RK45). The solution is obtained with use of script B.14 in Supplemental Material [33] (see the script for parameter values) and is compared with the solution obtained with use of script B.11, based on the singular value decomposition (SVD).

by sampling a sufficiently large number N of stochastic trajectories $\Psi_j = \{|\psi_j(t)\rangle\}$ to then obtain the time-evolved density operator $\rho(t)$ by averaging over them,

$$\rho(t) = \sum_{j=1}^{N} |\psi_j(t)\rangle\langle\psi_j(t)|. \tag{59}$$

Let H be the Hamiltonian of the system and let $\{L_k\}_{k=1}^{M}$ be a collection of Hermitian [91] Lindblad operators. In the simplest form of the method, each trajectory Ψ_j is sampled according to the following steps:

(1) The probabilities associated with any of the k incoherent transitions mediated by the L_k jump operators are calculated:

$$\delta p_k = \delta t \langle\psi(t)|L_k^\dagger L_k|\psi(t)\rangle \geq 0, \tag{60}$$

with $\delta p = \sum_{k=1}^{M} \delta p_k$.

(2) A uniform random number $u \in (0, 1]$ is sampled.

(a) If $\delta p < u$, then no jump occurs and the state $|\psi(t)\rangle$ at time t is evolved by means of the non-Hermitian effective Hamiltonian

$$H_{\text{eff}} = H - i\hbar \sum_{k=1}^{M} L_k^\dagger L_k/2 \tag{61}$$

to obtain

$$|\widetilde{\psi}(t+\delta t)\rangle = \left(1 - \frac{i}{\hbar} H_{\text{eff}}^\dagger \delta t\right)|\psi(t)\rangle, \tag{62}$$

where $|\widetilde{\psi}\rangle$ indicates that the state vector may not be normalized.

(b) If $\delta p \geq u$, a jump occurs. A new uniform random number $u' \in (0, 1]$ is sampled. The event that occurs is chosen by finding the first k such that $Q_k > u'$, where $Q_k = \sum_{j=1}^{k} \delta p_j / \delta p$. The state is propagated to be

$$|\widetilde{\psi}(t+\delta t)\rangle = L_k|\psi(t)\rangle. \tag{63}$$

(3) The state is normalized:

$$|\psi(t+\delta t)\rangle = \frac{|\widetilde{\psi}(t+\delta t)\rangle}{\sqrt{\langle\widetilde{\psi}(t+\delta t)|\widetilde{\psi}(t+\delta t)\rangle}}. \tag{64}$$

In this approach no superoperator is assembled and no matrix exponential is calculated. Furthermore, since the trajectories Ψ_j are completely independent of each other, this method can be trivially parallelized by one running N trajectories over N different processing nodes to reduce the computational time by a factor of N.

A PYTHON implementation is presented in script B.16 in Supplemental Material [33] for a two-level system with $H = \sigma_z$ and Lindblad operators $\{\sigma_z/2, \sigma_x/5\}$ with initial state $|\psi\rangle = (|0\rangle + |1\rangle)/\sqrt{2}$ in the σ_z basis. The results are shown in Fig. 9.

Note that the time-step δt can be chosen to be a fraction of some operator norm of the Hamiltonian, such that $\delta t \ll \|H\|_{\text{op}}^{-1}$. An equivalent MATHEMATICA implementation can be found in script C.9 in Supplemental Material [33]. A robust implementation of the stochastic wave function method is also available in QUTIP.

7. Time-dependent generators

If the Hamiltonian or the decoherence terms depend on time, Eq. (27) is generalized to

$$\dot{\boldsymbol{\rho}} = \mathcal{L}(t)\boldsymbol{\rho}, \tag{65}$$

where the Liouville generator $\mathcal{L}(t)$ now explicitly depends on time. In this case the solution of Eq. (35) is not valid.

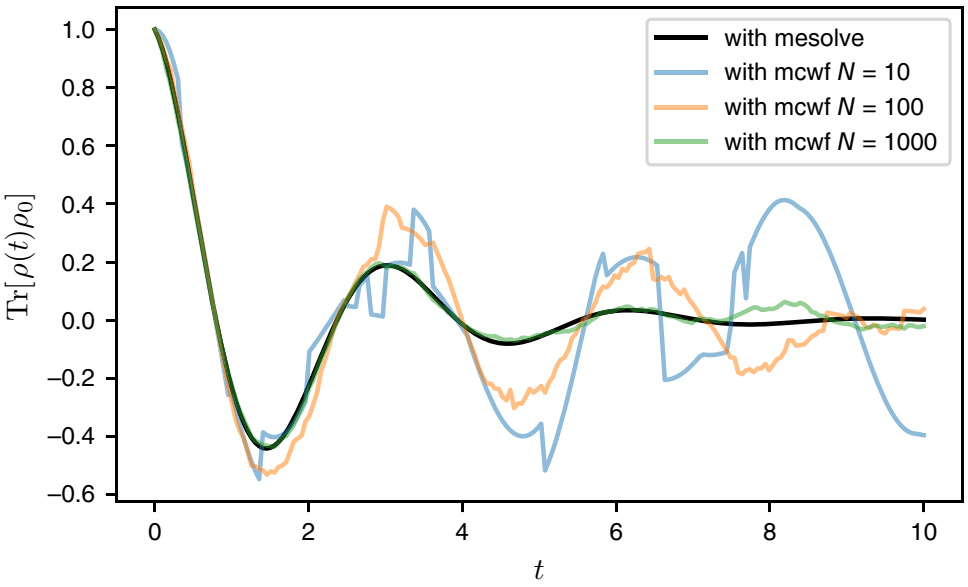

FIG. 9. Propagation with the stochastic wave function method with $N = 10$, 100, or 1000 trajectories using script B.16 in Supplemental Material [33] (see the script for parameter values), with `sample` $= N$. The stochastic wave function solution approaches the exact solution in the limit of large N. Here the solution is compared with the solution obtained with QUTIP's finite-difference method `mesolve`.

The general solution of Eq. (65) is given by

$$\boldsymbol{\rho}(t) = \mathcal{T}\left\{\exp\left[\int_0^t ds\mathcal{L}(s)\right]\right\}\boldsymbol{\rho}(t_0), \tag{66}$$

where $\mathcal{T}$ is the time-ordering operator, analogous to the Dyson series for time-dependent Hamiltonians and wave function propagation [26,92]. Equation (66) can be approximated, for instance, by means of a sequence of stepwise time-independent generators, before one resorts to other means of numerical integration.

If the generator $\mathcal{L}(t)$ is approximately *piecewise time independent*, then Eq. (35) can be applied to each time slice, with use of the result of the previous slice to provide the input state for the next slice. This scenario is common in many optical and spin resonance experiments. For example, it can be used to compute the effect of applying a laser pulse resonant with an atomic transition. It can then be used to model the behavior of the system while the pulse is ON and immediately after it is turned off.

Let us consider a system with Hamiltonian $H = H_0 + v(t)H_1$, where $H_0 = \omega_0\sigma_z/2$, $H_1 = \omega_0\sigma_x/2$, $v(t) = \cos(\omega t)$, and the Lindblad dephasing operator $J = |g\rangle\langle g| = (\mathbb{1} - \sigma_z)/2$, with dephasing rate γ. The generator $\mathcal{L}(t) = \mathcal{L}_0 + \mathcal{L}_1(t)$ can be split into a time-independent part $\mathcal{L}_0$, associated with H_0 and L_0, and a time-dependent part $\mathcal{L}_1(t)$. To reduce the computational cost when propagating this system, we can update the propagator by updating only the time-dependent part. The PYTHON script B.17 in Supplemental Material [33] generalizes the solution of Eq. (35) to the case of time-dependent generators by updating the superoperator at each time t; the solution is shown in Fig. 10.

Note that for this approach to be accurate, the time step δt has to be sufficiently small so that $v(t + \delta t) \approx v(t) + \mathcal{O}(\delta t^2)$. For rapidly varying time-dependent Hamiltonians, other methods are required. If $H(t)$ is periodic, a solution can be found with use of an effective time-independent Hamiltonian, obtained with use of Floquet theory, as discussed in Sec. V.

In practice, especially when one is using theoretical system parameters, it is often possible to get exact cancellations that may have no physical grounding but can result in degenerate eigenvectors. While there are mathematical techniques that deal with these situations, it is often easier to just add an infinitesimal (numerically of order machine precision) imaginary term $i\varepsilon$, $\varepsilon \ll 1$, to each element of the matrix. This can remove the degeneracy, even if the term is made sufficiently small to have no perceivable effect on the resulting calculations.

8. Sparse solvers and other methods

When one is dealing with very large systems, it is always desirable to exploit the sparseness of the superoperator and states, since calculating the matrix exponential and the singular value decomposition may become prohibitively expensive. Fortunately, most physical systems have sparse Liouvillians whose memory requirements scale as $d^2 2\ln(d)$. A number of different techniques can be used to treat sparse and large superoperators, such as the following:

(1) Use of methods for sparse arrays (`SparseArray` in MATHEMATICA), such as null-space solvers. A library of linear algebra methods for sparse arrays for MATLAB is available in Ref. [93];
(2) Use of Krylov subspace methods to solve for $\exp(\mathcal{L}t)\boldsymbol{\rho}_0$ directly [94]; the packages `expokitpy` and `KryPy` [95] offer Krylov method implementations for PYTHON.

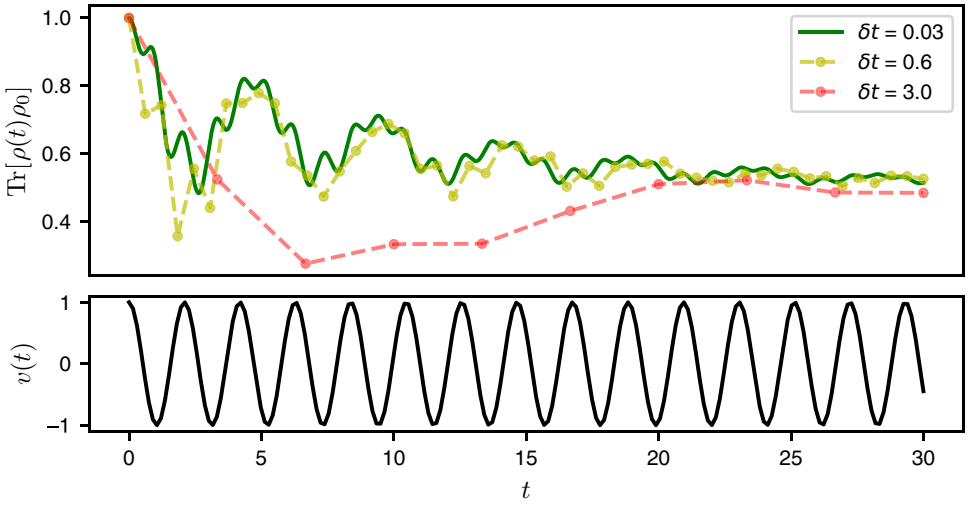

FIG. 10. Solution of time-dependent generator obtained with use of the piecewise time-independent propagator for the system considered in script B.17 in Supplemental Material [33] (see the script for parameter values). The evolution is generated by a time-dependent Hamiltonian $H(t) = \omega_0\sigma_z/2 + v(t)\omega_0\sigma_x/2$, with $v(t) = \cos(\omega t)$, and a time-independent Lindblad dephasing operator $J = (\mathbb{1} - \sigma_z)/2$, associated with rate γ. The solution is obtained for $\omega_0 = 2$, $\omega = 3$, and $\gamma = 0.3$ for three different time steps δt as indicated in the legend.

(3) Taking the action of the exponential on a given sparse initial state. In MATHEMATICA this can be done with `MatrixExp` as in

```
rhot = MatrixExp[M t, rho0]
```

(4) Use of the Arnoldi method [96]. This can be done in MATHEMATICA with use of the `Eigensystem` function in combination with `"Arnoldi"`,

```
Eigensystem[M t, k, Method ->
            "Arnoldi"]
```

where `k` represents the index of the eigenvalue (or singular value) to be calculated;

(5) Use of the Arnoldi-Lindblad method introduced in Ref. [97] for time-independent and periodically time-dependent systems. The method applies the Arnoldi iterative diagonalization while using the algebraic properties of the Liouville superoperator.

However, sometimes the simplest option may be to implement a finite-difference method such as the Runge-Kutta method with sparse linear algebra, as it is often just as fast as more sophisticated methods.

E. Correlation functions

Correlation functions measure the relationship between microscopic quantities across time, space, and other observables. In statistical mechanics, they are used to calculate the ensemble properties of stochastic processes and to determine the degree of order or randomness in a system. For example, the effect of atmospheric turbulence on the propagation of light beams can be modeled from the correlation functions $C(t, t', \mathbf{r}, \mathbf{r}') = \langle n(t, \mathbf{r}) n(t', \mathbf{r}') \rangle$ of the refractive index $n(t, \mathbf{r})$ [98]. Similarly, the magnetic properties of materials can be inferred from the spatial correlation functions between spins [99].

In quantum stochastic processes, correlation functions are used to determine the magnitude of decoherence and relaxation processes, as we discuss in depth in Sec. IV. The macroscopic properties of a variety of systems can be calculated from the correlation functions of their microscopic features. Of particular importance are emission and absorption spectra in light-matter interaction (see Sec. III E 2), noise power spectra and relaxation rates, and bunching and antibunching statistics of photons [100], electrons [101], and other particles. Here we examine the basics of correlation functions and show how these can be calculated from the master equation governing the evolution of the density operator. We then apply these results to calculate the emission spectrum in a simple example of a two-level system interacting with an electromagnetic field.

1. Quantum regression theorem

Linear systems are amply studied in physics because of their simplicity and exact solvability. The equations of motion of the averages of the operators of such systems are often linear, as for the case of Eq. (27). For these systems, it can be shown that the averages of their two-time correlation functions obey exactly the same equations of motion. This result, first derived by Lax, is known as the *quantum regression theorem* [102,103], and it provides a

method for calculating any two-time correlation function $\langle A(t)B(t')\rangle$, i.e., involving any two observables at different points in time, for a system whose dynamics are prescribed by a quantum master equation $\dot{\rho} = \mathcal{L}_t[\rho]$ [102].

Suppose that for a certain set of operators $\{A_i\}$, the linear master equation (27) yields the following closed system of linear ordinary differential equations to their averages for some coefficients G_{ij} [26]:

$$\frac{d}{dt}\langle A_i(t)\rangle = \sum_j G_{ij}\langle A_j(t)\rangle. \tag{67}$$

Then their two-point correlation functions

$$\langle A_i(t+\tau)A_l(t)\rangle = \mathrm{Tr}\big[A_i \Lambda(t+\tau;t)[A_l\rho(t)]\big], \tag{68}$$

where $\Lambda(t;t_0)$ is the dynamical map from time t_0 to time t, associated with the master equation $\dot{\rho} = \mathcal{L}_t[\rho]$ observe the same dynamics,

$$\frac{d}{dt}\langle A_i(t+\tau)A_l(t)\rangle = \sum_j G_{ij}\langle A_j(t+\tau)A_l(t)\rangle. \tag{69}$$

Note how the right-hand side of Eq. (68) corresponds to the average of A_i at time $t+\tau$ with the choice of initial density operator $\rho \to A_l\rho(t)$ [103].

Any two-time correlation function $\langle A(t+\tau)B(t)\rangle$ can then be simplified with use of Eq. (68) as [30]

$$\begin{aligned}\langle A(t+\tau)B(t)\rangle &= \mathrm{Tr}[A\Lambda(t+\tau;t)[B\rho(t)]\}],\\ &= \mathrm{Tr}[A\Lambda(t+\tau;t)[B\Lambda(t;0)[\rho(0)]]].\end{aligned} \tag{70}$$

When calculating $\langle A(t+\tau)B(t)\rangle$ numerically, we can first obtain $\rho(t) = \Lambda(t;0)[\rho(0)]$ with $\rho(0)$ as the initial state. We then propagate $B\rho(t)$ using the dynamical map, to obtain $\Lambda(t+\tau,t)[B\rho(t)]$, and conclude by taking the trace of the resulting operators. If we are interested in steady-state properties, the two-time correlation functions simplify further. By replacing $\rho(0)$ with the steady state $\rho_{\mathrm{SS}} = \lim_{t\to\infty}\Lambda(t;0)[\rho(0)]$, we can calculate $\langle A(t+\tau)B(t)\rangle$ as

$$\begin{aligned}\langle A(t+\tau)B(t)\rangle &= \mathrm{Tr}[A\Lambda(t+\tau;t)[B\rho_{\mathrm{SS}}]],\\ &= \mathrm{Tr}[A\Lambda(\tau;0)[B\rho_{\mathrm{SS}}]],\\ &= \langle A(\tau)B(0)\rangle.\end{aligned} \tag{71}$$

2. Emission and absorption spectra

Emission and absorption spectra of an optical material can be calculated from the two-time correlation functions of the transition operators associated with the emission and absorption of photons, respectively. For example, an atomic medium given by an ensemble of noninteracting d-level systems that interact with the electromagnetic field will emit light when excited. Its spectrally resolved intensity is proportional to its emission spectrum $E(\omega)$, which measures the likelihood of transition between eigenstates $|\phi_i\rangle \to |\phi_j\rangle$ with energy difference ω. In first-order perturbation theory, $E(\omega)$ can be calculated by means of the Fermi golden rule [26]. Line-broadening effects caused by decoherence and relaxation processes can be calculated in second-order perturbation theory with use of two-point correlation functions and the quantum regression theorem.

Let us consider a generic two-level emitter with Hamiltonian $H = \Omega\sigma_z/2$ to illustrate how the emission spectrum is calculated. The system can emit a photon via the transition operator $\sigma_- = (\sigma_x - i\sigma_y)/2$ and absorb a photon via its Hermitian conjugate $\sigma_-^\dagger = \sigma_+ = (\sigma_x + i\sigma_y)/2$. Let the system be in a stationary state ρ_{SS}. Then its emission spectrum is calculated from the correlation function of the transition operators $\langle\sigma_-^\dagger(\tau)\sigma_-(0)\rangle$ as [26]

$$E(\omega) \propto \mathcal{F}(\omega)[\langle\sigma_-^\dagger(\tau)\sigma_-(0)\rangle] \tag{72}$$

$$= \int_{-\infty}^{\infty} d\tau e^{-i\omega\tau}\langle\sigma_-^\dagger(\tau)\sigma_-(0)\rangle \tag{73}$$

$$= 2\,\mathrm{Re}\left\{\int_0^\infty d\tau e^{-i\omega\tau}\langle\sigma_-^\dagger(\tau)\sigma_-(0)\rangle\right\}, \tag{74}$$

where $\mathcal{F}(\omega)$ is the Fourier transform. Equation (74) follows from our decomposing the limits of the Fourier transform in Eq. (72) at $t = 0$, followed by the use of the relation $\langle\sigma_-^\dagger(-\tau_+)\sigma_-(0)\rangle = \langle\sigma_-^\dagger(\tau_+)\sigma_-(0)\rangle^*$, where τ_- denotes $\tau < 0$ and τ_+ denotes $\tau \geq 0$ [26]. The generalization to the emission spectra of multilevel emitters is obtained by generalization of Eq. (72) as discussed in Ref. [10]. The emission spectrum $E(\omega)$ is calculated as the sum of all the contributions from the possible transitions $|i\rangle \to |j\rangle$ between the eigenstates of the system with $i > j$, modeled by the operators $\sigma_{ij} = |\phi_j\rangle\langle\phi_i|$,

$$E(\omega) \propto \sum_{i>j}\mathcal{F}(\omega)[\langle J_{ij}^\dagger(\tau)J_{ij}(0)\rangle], \tag{75}$$

with $J_{ij} = \sqrt{\gamma_{ij}}\sigma_{ij}$, for some rates γ_{ij}.

If the emitter is illuminated by a tunable probe field with angular frequency ω_p, whose amplitude is assumed to be weak as to not significantly perturb the atom's Hamiltonian, the steady-state probe absorption spectrum can be obtained as follows [104–106]:

$$A(\nu) \propto \mathrm{Re}\left\{\int_0^\infty d\tau e^{i\nu\tau}\langle[\sigma_+^\dagger(\tau),\sigma_+(0)]\rangle\right\}, \tag{76}$$

where $\nu = \omega_p - \omega$ is the detuning of the probe beam relative to the driving laser.

We refer the reader to Refs. [1,107,108] for further details on correlation functions and spectra. We have

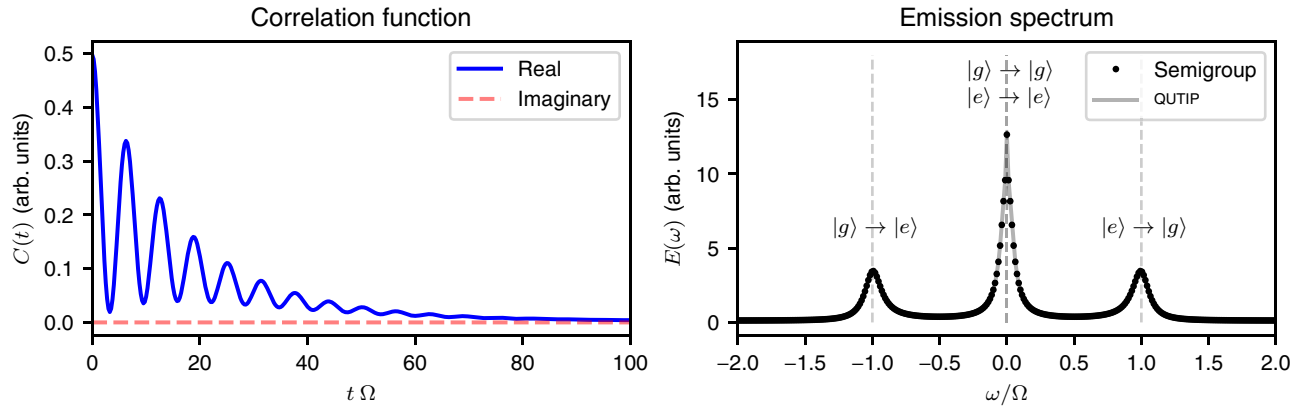

FIG. 11. Left: Real and imaginary parts of the steady-state correlation function $C(t) = \langle \sigma_+(\tau)\sigma_-(0)\rangle_{SS}$ for a two-level system $H = \Omega\sigma_z/2$ with Rabi frequency Ω and decay rate $\Gamma = \Omega/10$. Right: Emission spectrum $E(\omega)$ of the considered two-level system associated with transition operator $\sigma_- = |g\rangle\langle e| = \sigma_+^\dagger$. The peaks coincide with the transition frequencies $\omega_{ij} = \omega_i - \omega_j$ associated with transitions $|i\rangle \to |j\rangle$, as shown by the labels. The emission spectrum calculated with use of the semigroup composition rule is compared with the emission spectrum obtained with use of QUTIP with use of script C.10 in Supplemental Material [33] (see the script for parameter values).

included the step-by-step implementation of an example of a two-level system emission spectrum using Eq. (72) in script B.18 in Supplemental Material [33]. The resulting time-domain emission correlation and spectrum are depicted in Fig. 11, alongside the corresponding QUTIP version of the same calculation.

IV. BLOCH-REDFIELD THEORY

In the previous section we discussed how to implement the Lindblad master equation from a *phenomenological* model of decoherence and relaxation. However, it is sometimes necessary to start from a microscopic description—i.e., the system and environment Hamiltonian—to obtain a master equation for the density operator of the system. When the system interacts weakly with its environment, this can be achieved with use of Bloch-Redfield theory [26,109]. This theory is useful when we lack a model for decoherence and relaxation but we know the nature of the system-environment interactions that drive such processes. As a result, the theory provides a powerful approach to determine the temperature dependence of dephasing and thermalization rates directly from *first principles*.

A. Bloch-Redfield master equation

Let us consider a system S, with dimension $\dim_S$, that interacts with its environment E according to the following general Hamiltonian:

$$H = H_S + H_E + H_{\text{int}} \tag{77}$$

$$= H_S + H_E + \sum_\alpha A_\alpha \otimes B_\alpha, \tag{78}$$

where the coupling operators A_α (B_α) are Hermitian and act on the system (environment) such that H_{int} is a small perturbation of the unperturbed Hamiltonian $H_0 = H_S + H_E$. Then, under approximations 1–3 discussed in Sec. IV B, the dynamics of the system's density operator ρ in the eigenbasis $\{|\omega_a\rangle\}$ of H_S [110] is prescribed by the Bloch-Redfield master equation,

$$\dot\rho_{ab}(t) = -i\omega_{ab}\rho_{ab}(t) + \sum_{c,d} R_{abcd}\rho_{cd}(t), \tag{79}$$

where $\omega_{ab} = \omega_a - \omega_b$ are the frequencies associated with transitions $|\omega_b\rangle \to |\omega_a\rangle$. The Bloch-Redfield tensor R_{abcd} is prescribed by the following expression, where δ_{ij} is the Kronecker δ:

$$\begin{aligned} R_{abcd} = -\frac{1}{2\hbar^2}\sum_{\alpha,\beta}\Bigg\{ & \delta_{bd}\sum_{n=1}^{\dim_S} A^{(\alpha)}_{an}A^{(\beta)}_{nc}S_{\alpha\beta}(\omega_{cn}) \\ & - A^{(\alpha)}_{ac}A^{(\beta)}_{db}S_{\alpha\beta}(\omega_{ca}) \\ & + \delta_{ac}\sum_{n=1}^{\dim_S} A^{(\alpha)}_{dn}A^{(\beta)}_{nb}S_{\alpha\beta}(\omega_{dn}) \\ & - A^{(\alpha)}_{ac}A^{(\beta)}_{db}S_{\alpha\beta}(\omega_{db})\Bigg\}. \end{aligned} \tag{80}$$

In Eq. (80), $A^{(\alpha)}_{ab} = \langle\omega_a|A_\alpha|\omega_b\rangle$ are the elements of the coupling operators A_α in the eigenbasis of the system Hamiltonian, while $S_{\alpha\beta}(\omega)$ corresponds to the noise-power spectrum of the environment coupling operators [36,111],

$$S_{\alpha\beta}(\omega) = \int_{-\infty}^{\infty} d\tau e^{i\omega t}\,\text{Tr}\Big[B_\alpha(\tau)B_\beta(0)\rho_E\Big], \tag{81}$$

taken by our assuming ρ_E is some steady state of the environment.

1. Thermal relaxation and detailed balance condition

When Bloch-Redfield theory is used, it is common to consider environments in thermal equilibrium at inverse temperature $\beta = 1/k_B T$. For example, the environment may be assumed to be in a Bose-Einstein distribution,

$$G_\beta(H_E) = \frac{\exp(-\beta H_E)}{\mathcal{Z}}, \tag{82}$$

with $\mathcal{Z} = \mathrm{Tr}[\exp(-\beta H_E)]$, and to be invariant under future evolutions (Gibbs state) [26]. In the secular approximation, discussed in Sec. IV C, any out-of-equilibrium density operator that evolves under the dynamics prescribed by Eq. (79) with $\rho_E = G_\beta(H_E)$ will relax towards thermal equilibrium (exchanging energy with the environment). Indeed, the steady state of Eq. (79) is itself a Gibbs state $G_\beta(H_S)$ at thermal equilibrium with inverse temperature β.

The condition for this to occur is known as *detailed balance*, and can be expressed in terms of the ratio between the rates $k_{a\to b}$ associated with transitions $|\omega_a\rangle \to |\omega_b\rangle$ separated by energy $\omega_{ba} = \omega_b - \omega_a$:

$$\frac{k_{a\to b}}{k_{b\to a}} = \exp(-\beta\omega_{ba}). \tag{83}$$

The detailed balance condition implies that the equilibrium populations of the eigenstates of the system follow the Boltzmann distribution $p_a \propto \exp(-\beta\omega_a)$. In terms of noise-power spectra, the detailed balance condition becomes $S_{\alpha\beta}(-\omega)/S_{\alpha\beta}(\omega) = \exp(-\beta\omega)$.

2. Example: Spin-boson model

Before discussing the approximation required to derive the Bloch-Redfield master equation, let us implement Bloch-Redfield theory for the simple and ubiquitous spin-boson model. We consider a two-level system coupled with a large ensemble of *uncorrelated* harmonic oscillators at thermal equilibrium (bosonic bath)

$$H = \frac{\epsilon_0}{2}\sigma_z + \frac{\Delta}{2}\sigma_z + \sum_k \hbar\omega_k b_k^\dagger b_k + \sigma_z \otimes \sum_k g_k\left(b_k^\dagger + b_k\right), \tag{84}$$

where g_k is the strength of the coupling between σ_z and some mode ω_k.

First, we calculate the correlation functions $C_{kk'}(t)$ for the bath operators $B_k = g_k\left(b_k^\dagger + b_k\right)$,

$$C_{kk'}(t) = \delta_{kk'}\mathrm{Tr}\left[B_k(t)B_{k'}(0)G_\beta(H_E)\right], \tag{85}$$

$$= \frac{g_k^2}{1-\exp(-\beta\omega_k)}\left(e^{-i\omega_k t} + e^{i\omega_k t - \beta\omega_k}\right), \tag{86}$$

where we used the fact that the modes are uncorrelated ($\delta_{kk'}$) and assumed the bath to be in thermal equilibrium $\rho_E = G_\beta(H_E)$ at inverse temperature β, as in Eq. (82).

To treat the contribution of a large ensemble of modes, we replace the sum over the coupling strength g_k with an integral over some spectral density $J(\omega)$ that well approximates the bath:

$$\sum_k g_k^2 \to \int_0^\infty d\omega J(\omega). \tag{87}$$

The spectral density is the product of the square of the system-environment coupling strength and the density of environmental states in frequency space [112]. A common choice is the Ohmic spectral density $J(\omega) = \eta\omega e^{-\omega/\omega_c}$, which is characterized by a cutoff frequency ω_c and a dimensionless parameter η, from which we obtain the noise-power [69],

$$S(\omega) = \int_{-\infty}^\infty dt e^{i\omega t}\sum_k C_{kk}(t) \tag{88}$$

$$\approx \int_{-\infty}^\infty dt e^{i\omega t}\int_0^\infty d\omega' J(\omega')\frac{\left(e^{-i\omega' t} + e^{i\omega' t - \beta\omega'}\right)}{1-\exp(-\beta\omega')} \tag{89}$$

$$= \frac{2\pi\eta\omega\exp(-|\omega|/\omega_c)}{1-\exp(-\beta\omega)}. \tag{90}$$

We now possess all the elements required to compose the Bloch-Redfield tensor of Eq. (80). Note that we have only one system coupling operator $A = \sigma_z$, associated with a single noise-power spectrum $S(\omega)$. The PYTHON script B.19 in Supplemental Material [33] presents an implementation of the Bloch-Redfield tensor, which can then be used to propagate the state of the system with use of one of the methods discussed in Sec. III. Note that to simplify the solution of Eq. (27), the unitary part of the generator has been absorbed into the tensor R,

$$R_{abcd} \to R'_{abcd} = -i\omega_{ac}\delta_{ac}\delta_{bd} + R_{abcd}. \tag{91}$$

B. Approximations for the Bloch-Redfield master equation

While the Lindblad master equation is guaranteed to be completely positive and trace preserving [113], care must be taken when one is using Bloch-Redfield theory.

First, the following approximations have to be respected to obtain Eq. (79) from the reduced-state von Neumann equation [26,109], as discussed in Sec. II E:

(1) *Weak-coupling approximation.* The interaction $H_{\rm int}$ is a small perturbation of the unperturbed Hamiltonian $H_0 = H_S + H_E$.
(2) *Born approximation.* The system-environment density operator is factorized at all times, $\rho_{\rm int}(t) = \rho_S(t) \otimes \rho_E$, with ρ_E being some steady state of the environment (justified also by the weak-coupling approximation).
(3) *Markov approximation.* The bath correlation functions $g_{\alpha\beta}(\tau) = {\rm Tr}\big[B_\alpha(\tau)B_\beta(0)\rho_E\big]$ have a short correlation timescale τ_E, $g_{\alpha\beta}(\tau) \approx 0$ for $\tau \gg \tau_E$.

Within these approximations, the Bloch-Redfield master equation does not, in principle, guarantee positivity of the density operator. That is, when one is propagating the system in time $\rho(t) = \Lambda_t[\rho_0]$, the populations of ρ may become negative for some time $t > 0$ [114]. For this reason, when one is propagating a density operator numerically, it is advisable to check its positivity. The PYTHON script B.20 in Supplemental Material [33] can be used to test the positivity, Hermitianity, and normalization condition of a density operator. The function `is_state(rho)` returns 1 if a `rho` is a density operator and a value $s < 1$ if `rho` deviates from the conditions of positivity, Hermitianity, and normalization, where $1 - s$ is a measure of such deviation.

C. Lindblad form of the Bloch-Redfield master equation

By application of the rotating-wave approximation (RWA), it is possible to write the Bloch-Redfield master equation in the Lindblad form of Eq. (24) and thus guarantee its complete positivity,

$$\dot\rho = -\frac{i}{\hbar}[H_S,\rho] + \sum_{\alpha\beta}\sum_{\omega} S_{\alpha\beta}(\omega)\Big[A_\alpha(\omega)\rho A_\beta^\dagger(\omega) - \frac{1}{2}\Big\{A_\alpha^\dagger(\omega)A_\beta(\omega),\rho\Big\}\Big], \tag{92}$$

where $A_\alpha(\omega) = \sum_{\omega=\omega_b-\omega_a} A_{ab}^{(\alpha)}|\omega_a\rangle\langle\omega_b|$ are the coupling operators in the frequency domain, such that the sum over ω needs to be done only over the transition (Bohr) frequencies $\omega = \omega_b - \omega_a$, as in Eq. (80) [26]. To apply the RWA, all the contributions from the rapidly oscillating terms, i.e., with characteristic frequency $|\omega_{ab} - \omega_{cd}| \geq \tau_E^{-1}$, are ignored as they approximately average to zero. This is sometimes also called "secular approximation," although technically the two approximations do not coincide [115].

This form is useful, for example, to systematically compile the Bloch-Redfield tensor from a list of system coupling operators A_α and noise-power spectra $S_{\alpha\alpha}$, or even to compose the full Liouville superoperator associated with the dynamics of Eq. (92).

Example: Network with random energies and couplings. Let us consider a system consisting of N states $|k\rangle$ with energies ε_k that interact via couplings v_{jk}, with associated Hamiltonian

$$H_S = \sum_k \varepsilon_k|k\rangle\langle k| + \sum_{j<k}\Big(v_{jk}|j\rangle\langle k| + {\rm h.c.}\Big). \tag{93}$$

Let us assume that each state $|k\rangle$ couples with a local environment of uncorrelated bosonic modes characterized by some noise-power spectrum $S_k(\omega)$. This type of system-environment model is typically used to model the transport of charge carriers (electrons and holes) or coupled electron-hole pairs (*excitons*) in disordered organic semiconductors [116]. In the PYTHON script B.21 in Supplemental Material [33] we study the dynamics of an instance of such a random quantum network using Bloch-Redfield theory in the secular approximation; the results are shown in Fig. 12.

The Bloch-Redfield tensor is calculated with use of the general method introduced in script B.19 in Supplemental Material [33], while the propagator is calculated adaptively for different timescales. A robust and efficient method for the calculation of the Bloch-Redfield tensor is implemented in the `bloch_redfield_tensor` function of QUTIP's module `bloch_redfield`.

D. Computational requirements for the Bloch-Redfield master equation

Numerical implementations of Markovian master equations such as the Lindblad and Bloch-Redfield master equations are generally inexpensive, when compared with the numerical implementation of methods involving memory kernels or environmental degrees of freedom [26,117]. Nevertheless, as the size of the system increases, solving density operator master equations can become computationally demanding [118]. Therefore, when one is implementing Bloch-Redfield theory numerically, it is important to keep track of the required computational resources.

1. Memory requirements

Let $d = \dim\mathcal{H}_S$ be the dimension of the Hilbert space associated with the system's Hamiltonian H_S. For any density operator master equation, the number of complex floating-point numbers required to store the density operator scales with d^2, with the coherences (off-diagonal elements) taking up most of this memory requirement.

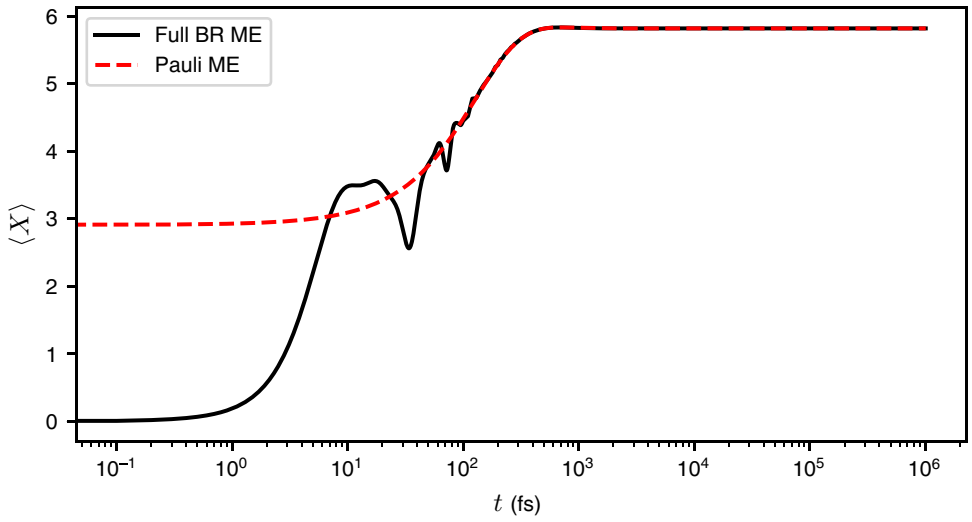

FIG. 12. Solution of the Bloch-Redfield (BR) master equation (ME) and associated Pauli master equations for the random quantum network of scripts B.21 and B.22 in Supplemental Material [33] (see the scripts for parameter values).

Analogously, the memory requirements to store the Liouville superoperator associated with Eqs. (24) and (79) scale as d^4. When memory becomes an issue, it is possible to use *stochastic wave function* methods to limit the memory scaling to that of the system dimension (d) for the state and that of the Hamiltonian (d^2) for the propagation, as discussed in Sec. III D 6.

2. Operations requirements

There are three main computationally demanding tasks one encounters when solving any density operator master equation numerically in Liouville space:

(1) Constructing the generator of the evolution $\mathcal{L}$, associated with $\dot{\boldsymbol{\rho}} = \mathcal{L}\boldsymbol{\rho}$.
(2) Computing the propagator $P_t = \exp[\mathcal{L}t]$.
(3) Propagating the state $\boldsymbol{\rho}_t = P_t\boldsymbol{\rho}_0$.

As discussed in Sec. III D, there is an array of approaches to reduce the expense of these tasks, depending on the type of problem.

a. Propagation. Starting from the bottom, propagating the state in Liouville space involves a matrix multiplication $P\boldsymbol{\rho}$ between a d^2 vector $\boldsymbol{\rho} = \mathrm{vec}(\rho)$ and a $d^2 \times d^2$ operator P. Without any optimization, the number of floating-point operations required scales with d^4 [118].

b. Matrix exponential. The number of operations required to compute the propagator depends on the method used to calculate the exponential of the matrix associated with $\mathcal{L}$. For example, SCIPY's implementation (`scipy.linalg.expm`) uses the Padé method to approximate the matrix exponential (see Refs. [119,120] for details on the number of operations required). This is generally a demanding task, for Lindblad and Bloch-Redfield master equations alike. Some approaches to mitigate the computational costs associated with this task are discussed in Sec. III D.

c. Bloch-Redfield tensor. When it comes to constructing the generator of the evolution, calculating the Bloch-Redfield tensor R becomes substantially more demanding than calculating the bare Lindblad generator $\mathcal{L}$. In essence, this is because each system coupling operator A_α may contribute to any of the d^2 transitions $|\omega_a\rangle\langle\omega_b|$ in the eigenbasis of H_S. Therefore, when constructing a Bloch-Redfield tensor from m coupling operators A_α, we may need to perform a number of operations that scales with $m^2 \times d^2$. In contrast, to construct a Lindblad superoperator $\mathcal{L}$ from m *jump* operators L_k, we need a number of operations that scales only with m. See Ref. [118] for further information on the computational resources required for Bloch-Redfield theory and the efficiency of different numerical implementations. It is worth mentioning that the numerical construction of the Bloch-Redfield tensor for time-dependent Hamiltonians can become particularly challenging, as it is often necessary to reconstruct the tensor as the Hamiltonian eigensystem changes over time.

E. Pauli master equation

The computational cost of Bloch-Redfield master equations reduces dramatically under some special circumstances. If the system's Hamiltonian H_S is nondegenerate

and if the secular approximation is applied [121], the equations of motion for the populations $p_a(t)$ of the eigenstates $|\omega_a\rangle$ are closed and decoupled from the equations of motion for the coherences [26]. The result is a system of linear ordinary differential equations to the populations, known as the Pauli master equation:

$$\dot{p}_a(t) = \sum_b \left[W_{ab}p_b(t) - W_{ba}p_a(t)\right], \tag{94}$$

where the matrix elements

$$W_{ab} = \sum_{\alpha\beta} A^{(\alpha)}_{ba} A^{(\beta)}_{ab} S_{\alpha\beta}(\omega_{ba}) \tag{95}$$

represent the rates of transition between eigenstates a and b.

The Pauli equation (94) can be written in the vector form $\dot{\mathbf{p}}(t) = W\mathbf{p}(t)$ and solved analytically or numerically with use of the matrix exponential $\mathbf{p}(t) = \exp[Wt]\mathbf{p}(0)$. Since the population vector $\mathbf{p}$ is d dimensional, the computational resources required to implement the Pauli master equation scale with d^2. Pauli master equations find applications in scenarios where dephasing happens over a much shorter timescale than thermal relaxation. As an example, room-temperature exciton transport properties were studied with this approach in Refs. [122,123]. Script B.22 in Supplemental Material [33] implements the Pauli master equation associated with the problem set up in script B.21. The results are shown in Fig. 12.

V. PERIODICALLY DRIVEN SYSTEMS AND FLOQUET THEORY

Up until this point, all the Hamiltonians considered are constant, are piecewise constant, or vary slowly enough that they can be considered piecewise constant. Now we consider the common situation where some part of the Hamiltonian is periodically oscillating in time:

$$H(t) = H_0 + \sin(\omega t + \phi_0)H_1, \tag{96}$$

where H_0 and H_1 are two (generally noncommuting) time-independent Hamiltonians, ω is some oscillation frequency, and $\phi_0 \in \mathbb{R}$ is some initial phase. A very common example is a two-level system interacting with an oscillating electric or magnetic field, which is encountered experimentally when one is driving transitions with a laser or a microwave field. However, the approach detailed here is very general and applies to any harmonically oscillating Hamiltonian whose frequency ω and overtones $k\omega$ ($k \in \mathbb{Z}$) are near resonant with a transition $|E_n\rangle \to |E_m\rangle$ between eigenstates $|E_n\rangle$ with energy E_n of the considered internal Hamiltonian H_0,

$$k\hbar\omega \approx |E_m - E_n|. \tag{97}$$

A. Two-level system interacting with an electric field

Let us consider a single two-level system subjected to an oscillating electric field $\mathbf{E}(t)$ of wavelength λ. If the atom is much smaller than λ, the field will appear spatially constant in the region occupied by the atom. This enables us to write the field as a function of time,

$$\mathbf{E}(t) = \left(E_0 e^{-i\omega t} + E_0^* e^{i\omega t}\right)\hat{z}, \tag{98}$$

assuming that $\mathbf{E}$ is oriented along the $\hat{z}$ direction, where ω is the angular frequency of the incoming radiation.

The total system Hamiltonian $H = H_S + H_{\text{int}}$ is the sum of the Hamiltonian of the two-level system,

$$H_S = \hbar\frac{\omega_0}{2}\sigma_z, \tag{99}$$

with eigenstates $|g\rangle$ and $|e\rangle$, and the atom-field dipolar interaction Hamiltonian H_{int} [124,125],

$$H_{\text{int}} = -\mathbf{d}\cdot\mathbf{E}, \tag{100}$$

where $\mathbf{d}$ is the transition dipole moment operator of the atom. Assuming that the field predominantly interacts with only one electron in the atom, we write $\mathbf{d}$ in terms of the electron position $\mathbf{r}_e$ as $\mathbf{d} = -e\mathbf{r}_e$, where e is the elementary charge. With use of a parity argument, it can be shown that the diagonal matrix elements of $\mathbf{d}$ vanish, i.e., $\langle g|\mathbf{d}|g\rangle = \langle e|\mathbf{d}|e\rangle = 0$. As a result, the dipole operator reads

$$\mathbf{d} = \langle e|\mathbf{d}|g\rangle|e\rangle\langle g| + \langle e|\mathbf{d}|g\rangle^*|g\rangle\langle e|, \tag{101}$$

from which we define the Rabi frequency Ω of the two-level system and its associated *counter-rotating* frequency $\widetilde{\Omega}$,

$$\Omega = \langle g|\mathbf{d}\cdot\hat{z}|e\rangle\frac{E_0}{\hbar}, \quad \widetilde{\Omega} = \langle e|\mathbf{d}\cdot\hat{z}|g\rangle\frac{E_0^*}{\hbar}. \tag{102}$$

The interaction Hamiltonian then reads

$$\begin{aligned} H_{\text{int}} = &-\hbar\left(\Omega e^{-i\omega t} + \widetilde{\Omega}e^{i\omega t}\right)|e\rangle\langle g| \\ &- \hbar\left(\widetilde{\Omega}^* e^{-i\omega t} + \Omega^* e^{i\omega t}\right)|g\rangle\langle e|. \end{aligned} \tag{103}$$

1. Rotating-wave approximation

Let us now write the full Hamiltonian H in the interaction picture $\widetilde{H} = U_0^\dagger H U_0$, with $U_0 = \exp(-iH_S t/\hbar)$,

$$\begin{aligned} \widetilde{H} = H_S &- \hbar\left(\Omega e^{-i\Delta\omega t} + \widetilde{\Omega}e^{i(\omega+\omega_0)t}\right)|e\rangle\langle g| \\ &- \hbar\left(\widetilde{\Omega}^* e^{-i(\omega+\omega_0)t} + \Omega^* e^{i\Delta\omega t}\right)|g\rangle\langle e|, \end{aligned} \tag{104}$$

with $\Delta\omega = \omega - \omega_0$. If the driving field is close to resonance with the energy splitting of the two-level system,

i.e., $\omega \approx \omega_0$, the two timescales involved in the dynamics are separated from each other,

$$\Delta\omega \ll \omega + \omega_0. \tag{105}$$

The rapidly oscillating terms in $\omega + \omega_0$, associated with the counter-rotating frequency $\widetilde{\Omega}$, quickly average to zero over the timescale of the Rabi frequency Ω. As a result, the RWA of the Hamiltonian H in the original frame reads

$$H^{\mathrm{RWA}} = H_S - \hbar\Big(\Omega e^{-i\omega t}|e\rangle\langle g| + \Omega^* e^{i\omega t}|g\rangle\langle e|\Big). \tag{106}$$

2. Time-independent Hamiltonian in the rotating frame

The Hamiltonian in Eq. (106) can be written in the rotating frame of the driving field via the transformation generated by the time-dependent unitary $V_\omega = \exp(iH_S t/\hbar) = \exp(i\omega\sigma_z/2t)$ [124],

$$H^{\mathrm{RWA}} \to H_\omega^{\mathrm{RWA}} = V_\omega H {V_\omega}^\dagger + i\hbar \dot{V}_\omega {V_\omega}^\dagger. \tag{107}$$

In this frame the Hamiltonian reads

$$\begin{aligned} H_\omega^{\mathrm{RWA}} &= \hbar\frac{\Delta\omega}{2}\sigma_z + \hbar\mathrm{Re}[\Omega]\sigma_x + \hbar\mathrm{Im}[\Omega]\sigma_y, \\ &= \frac{\hbar}{2}\begin{pmatrix} \Delta\omega & 2\Omega^* \\ 2\Omega & -\Delta\omega \end{pmatrix}. \end{aligned} \tag{108}$$

This is now a time-independent Hamiltonian in the rotating frame of the driving field, and can be treated with the methods introduced in previous sections. Typically, the decoherence operators are not oscillatory and are also time independent in this frame, which means solving the master equation also proceeds as above.

B. Floquet theory and Schrödinger evolution

The RWA is strictly valid only when the Rabi frequency Ω is much smaller than the transition frequency ω_0. When this is not the case, for example, in the limit of strong driving inducing multiphoton processes, more sophisticated techniques are required [126].

A common approach to treating strong driving beyond the RWA is the use of Floquet theory. In this approach, the evolution of a system undergoing periodic variation is expressed in a Fourier series in terms of the oscillation frequency. The Floquet theorem states that a set of time-dependent differential equations whose coefficients vary periodically will have solutions with the same periodicity. This is the temporal equivalent of Bloch's theorem in space, with the solution expressed in terms of quasienergies instead of quasimomenta.

In the context of quantum systems, Floquet theory provides a method for finding solutions to the time-dependent Schrödinger equation due to the influence of a time-periodic Hamiltonian. The Floquet treatment of the two-level system problem under strong driving was introduced by Shirley [127]. However, the approach is of general validity and is invaluable in a variety of settings, such as analogue quantum simulation [128], quantum information processing [129], heat engines and laser cooling [130], quantum optimal control [131,132], and time crystals [133,134].

1. Floquet modes and quasienergies

Let us consider the time-dependent Schrödinger equation for a periodic Hamiltonian $H(t) = H(t + nT)$, for all $n \in \mathbb{Z}$,

$$i\hbar\frac{d}{dt}|\psi(t)\rangle = H(t)|\psi(t)\rangle. \tag{109}$$

The Floquet theorem states that the general solution has the form

$$|\psi(t)\rangle = \sum_\alpha e^{-i\epsilon_\alpha t/\hbar}|\phi_\alpha(t)\rangle, \tag{110}$$

where $|\phi_\alpha(t)\rangle = |\phi_\alpha(t + nT)\rangle$ are some periodic functions, known as *Floquet modes*, and ϵ_α are the associated quasienergies, constant in time and uniquely defined up to multiples of $\omega = 2\pi/T$ [127]. By plugging Eq. (110) into Eq. (109), we can recast the problem as an eigenvalue problem to the quasienergies for the operator $H(t) := H(t) - i\hbar d_t$,

$$H(t)|\phi_\alpha(t)\rangle = \epsilon_\alpha|\phi_\alpha(t)\rangle. \tag{111}$$

This equation can be solved numerically or analytically to find the quasienergies and the Floquet modes. An alternative approach to finding the solution is to solve the eigenvalue problem posed by the propagator $U(t + nT; t)$ [135],

$$U(t + nT; t)|\phi_\alpha(t)\rangle = e^{-i\epsilon_\alpha T/\hbar}|\phi_\alpha(t)\rangle, \tag{112}$$

which is then solved for $\eta_\alpha = \exp(-i\varepsilon_\alpha T/\hbar)$, to find $\varepsilon_\alpha = -\hbar\arg(\eta_\alpha)/T$. This approach is implemented in QUTIP with the `floquet_modes` method.

2. Floquet Hamiltonian and Fourier analysis

Thanks to their shared periodicity we can express both the Hamiltonian and the Floquet modes as Fourier series,

$$|\phi_\alpha(t)\rangle = \sum_n e^{-i\omega nt}|\alpha, n\rangle, \tag{113}$$

$$H(t) = \sum_n e^{-i\omega nt}H_n, \tag{114}$$

where we have implicitly introduced the Fourier components $|\alpha, n\rangle$ and H_n of the Floquet modes and of the

Hamiltonian, respectively,

$$|\alpha, n\rangle = \frac{1}{T}\int_0^T dt e^{i\omega n t}|\phi_\alpha(t)\rangle, \tag{115}$$

$$H_n = \frac{1}{T}\int_0^T dt e^{i\omega n t} H(t). \tag{116}$$

This allows us to define a *Floquet Hamiltonian* H_F whose components are given by

$$\langle \alpha, n|H_F|\beta, m\rangle = H_{n-m}^{(\alpha,\beta)} + n\omega\delta_{\alpha\beta}\delta_{nm}, \tag{117}$$

which can be used to calculate probabilities of transition $P_{\alpha\to\beta}(t)$ between modes α and β, as discussed in the next section.

3. Transition probabilities from Floquet theory

Let us consider a simple sinusoidal variation in the Hamiltonian, such that H has a finite Fourier series

$$H(t) = \sum_{n=-1}^{1} e^{-i\omega n t} H_n, \tag{118}$$

$$= H_0 + \widetilde{H}_1 \cos(\omega t), \tag{119}$$

with $\widetilde{H}_1 := H_{-1}e^{-i\omega t} + H_1 e^{i\omega t}$. Then the Floquet Hamiltonian has the general structure

$$H_F = \begin{pmatrix} H_0 - 2\hbar\omega & H_1 & 0 & 0 & 0 \\ H_{-1} & H_0 - \hbar\omega & H_1 & 0 & 0 \\ 0 & H_{-1} & H_0 & H_1 & 0 \\ 0 & 0 & H_{-1} & H_0 + \hbar\omega & H_1 \\ 0 & 0 & 0 & H_{-1} & H_0 + 2\hbar\omega \end{pmatrix}, \tag{120}$$

where the size of the matrix is limited by the number of harmonics included in the Fourier expansion. If we then diagonalize H_F, the time-dependent wave function can be written in terms of the eigenvectors $|\lambda\rangle$ and corresponding

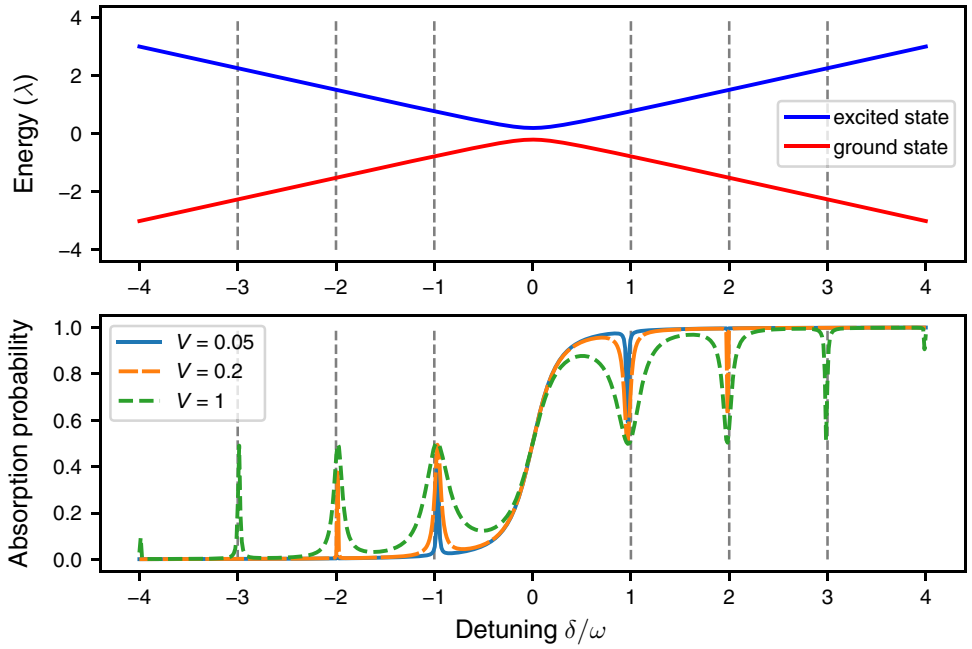

FIG. 13. Absorption probability associated with the transition $|g\rangle \to |e\rangle$ in a two-level system with Hamiltonian $H_0 = \delta\sigma_z/2 + \varepsilon\sigma_x$ and eigenvalues λ_g and λ_e. The system is strongly driven via the interaction $H_{\text{int}} = V\sigma_z/2$ with a cavity mode of frequency ω. The vertical dashed lines correspond to the n-photon transitions, which are enabled as the interaction strength V increases. The figures are generated with use of script C.11 in Supplemental Material [33] (see the script for parameter values).

eigenvalues λ of the Floquet Hamiltonian:

$$H_F|\lambda\rangle = \lambda|\lambda\rangle. \tag{121}$$

The time-dependent wave function $|\psi(t)\rangle = U(t;t_0)|\psi(t_0)\rangle$ is then expressed in terms of the propagator $U(t;t_0)$, whose elements can be written as

$$\begin{aligned} U_{\beta\alpha}(t;t_0) &= \sum_n \langle\beta,n|\exp[-iH_F(t-t_0)/\hbar]|\alpha,0\rangle e^{in\omega t} \\ &= \sum_n \sum_\lambda \langle\beta,n|\lambda\rangle\langle\lambda|\alpha,0\rangle e^{-i\lambda(t-t_0)/\hbar} e^{in\omega t}. \end{aligned} \tag{122}$$

The probability at time t of a given transition $\alpha \to \beta$ between Floquet modes with quasienergies ϵ_α and ϵ_β can then be computed directly:

$$P_{\alpha\to\beta}(t-t_0) = \sum_k |\langle\beta k|\exp[-iH_F(t-t_0)/\hbar]|\alpha 0\rangle|^2. \tag{123}$$

In addition, because the time evolution is given by the Floquet components, the time-averaged probability $\overline{P}_{\alpha\to\beta}$ can be evaluated as

$$\overline{P}_{\alpha\to\beta} = \sum_k \sum_\lambda |\langle\beta k|\lambda\rangle\langle\lambda|\alpha 0\rangle|^2. \tag{124}$$

This equation is implemented in the PYTHON script B.23 in Supplemental Material [33] for a system given by a two-level system interacting with a quantized electromagnetic field mode $a^\dagger$ with frequency ω,

$$H = H_S + V\sigma_z(a^\dagger e^{-i\omega t} + a e^{i\omega t}) + \hbar\omega a^\dagger a, \tag{125}$$

under different driving strengths V, as shown in Fig. 13.

The size of the Floquet Hamiltonian scales with both the number of states and the number of modes included in the Floquet expansion. The relative magnitude of $||H_1||$ to $||H_0||$ controls how many modes need to be included. In practice, this can be determined by one increasing the number of modes until the result converges. It is worth noting that this method can be computationally costly due to the size of the Floquet Hamiltonian. However, if convergence can be achieved, the method is *exact* and therefore can be used to compute the effects of strong driving, multiphoton transitions, and other effects beyond the rotating-wave approximation.

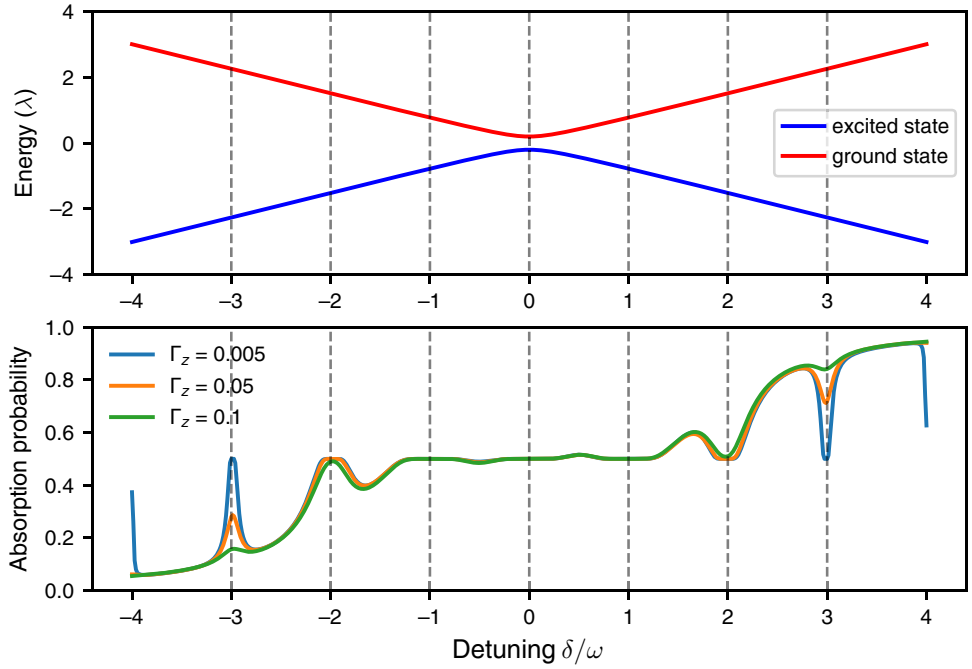

FIG. 14. Absorption probability associated with the transition $|g\rangle \to |e\rangle$ in a two-level system with Hamiltonian $H_0 = \delta\sigma_z/2 + \varepsilon\sigma_x$ and eigenvalues λ_g and λ_e. The system is strongly driven via the interaction $H_{\text{int}} = V\sigma_z/2$ with a cavity mode of frequency ω, while also being affected by the dephasing Lindblad operator $L = \sigma_z$ at rate Γ_z. The vertical dashed lines correspond to the n-photon transitions, which are damped as the dephasing rate increases. The figures are generated with use of script B.24 in Supplemental Material [33] (see the script for parameter values).

4. Extension of Floquet theory to decoherence processes

While the extension of Shirley's approach to model decoherence is less well established, there have been a number of different approaches, depending on how the expansion in Floquet components is introduced in the master equation [92,136–138] as well as other approaches to including beyond-rotating-wave physics into a master equation treatment [126,139–142].

One approach, which is also relatively simple to code, was introduced by Bain and Dumont [143] to model higher-order corrections in magic angle spinning NMR experiments. In their approach they use the Liouville form introduced in Sec. III B and express a periodic superoperator $\mathcal{L}_t$ as a Floquet expansion,

$$\mathcal{L}_t = \sum_{n=-\infty}^{\infty} e^{-in\omega_t} \mathcal{L}^{(n)}, \tag{126}$$

resulting in a *Floquet superoperator* $\mathcal{L}_F$,

$$\mathcal{L}_F = \begin{pmatrix} \cdots & \cdots & \cdots & \cdots & \cdots & \cdots & \cdots \\ \cdots & \mathcal{L}^{(0)} - 2\hbar\omega & \mathcal{L}^{(1)} & 0 & 0 & 0 & \cdots \\ \cdots & \mathcal{L}^{(-1)} & \mathcal{L}^{(0)} - \hbar\omega & \mathcal{L}^{(1)} & 0 & 0 & \cdots \\ \cdots & 0 & \mathcal{L}^{(-1)} & \mathcal{L}^{(0)} & \mathcal{L}^{(1)} & 0 & \cdots \\ \cdots & 0 & 0 & \mathcal{L}^{(-1)} & \mathcal{L}^{(0)} + \hbar\omega & \mathcal{L}^{(1)} & \cdots \\ \cdots & 0 & 0 & 0 & \mathcal{L}^{(-1)} & \mathcal{L}^{(0)} + 2\hbar\omega & \cdots \\ \cdots & \cdots & \cdots & \cdots & \cdots & \cdots & \cdots \end{pmatrix}, \tag{127}$$

that generates the dynamics in an effective time-independent Markovian master equation, in analogy with the Floquet Hamiltonian in the Shirley approach. To illustrate this approach, we have included a step-by-step implementation of the Floquet superoperator (script B.24 in Supplemental Material [33]) and an example of its use for a driven two-level system with decoherence (script C.12 in Supplemental Material [33]), as shown in Fig. 14.

However, the existence of a time-independent Floquet superoperator $\mathcal{L}_F$ is not always guaranteed, as shown in Ref. [92]. Depending on the choice of $\mathcal{L}_t$, the evolution might be described by an equivalent non-Markovian master equation that is homogeneous in time but not time local. Although more computationally demanding than the standard Floquet approach, this extension to decoherence processes is quite general and can be applied to master equations with oscillatory Hamiltonian components fairly easily [144,145].

VI. DISCUSSION

In this tutorial we have covered the basics of quantum master equations, showcasing their significance with examples and discussions. The methods reviewed here, such as use of the GKSL master equation and Bloch-Redfield theory are the cornerstone of stochastic quantum dynamics, and constitute only a small fraction of the developed field of open quantum systems. For further reading on these topics, we direct readers to Refs. [26,36,38,41,54,64,79,103,146–150]. The power of quantum master equations goes well beyond the systems and examples considered. The theory has been extended to non-Markovian dynamics [151–156], nonlinear systems [157,158], and time-convolutionless master equations [159–162], and is in constant development [163–168].

Further research in this field has been focusing on several aspects, such as extending the applicability of QMEs beyond the standard approximations [114,169,170], the combination of use of QMEs with compression methods [171] such as tensor networks [172–177], the use of neural networks [178–181], and the quantum simulation of open system dynamics [182–185]. These exciting developments are set to expand the range of applicability of QMEs to problems that are typically hard to solve, such as the dynamics of correlated many-body quantum systems that underlie the physics of quantum phase transitions [186–190], quantum computing architectures [191–194], optoelectronic devices [195,196], and complex chemical reactions [197–200].

ACKNOWLEDGMENTS

The authors acknowledge the Australian Research Council (Grant No. CE170100026) for funding and the National Computational Infrastructure, supported by the Australian Government, for computational resources. H.H. gratefully acknowledges Dinuka U. Kudavithana for insightful discussions. F.C. acknowledges that the work reported in this tutorial received funding from the European Union Horizon Europe research and innovation program under the Marie Skłodowska-Curie Action for the

project SpinSC. J.H.C. thanks A. Greentree, J. Ang, S. André, C. Müller, J. Jeske, N. Vogt, J. Vaitkus, and any other collaborators I've forgotten for useful input and corrections over the 15 years we used the set of technical notes on superoperators that were the inspiration for this tutorial.

[1] H. J. Carmichael, *Statistical Methods in Quantum Optics 1. Master Equations and Fokker-Planck Equations*, Theoretical and Mathematical Physics (Springer Berlin Heidelberg, Berlin, Heidelberg, 1999), 1st ed.

[2] P. W. Atkins and G. T. Evans, Electron spin polarization in a rotating triplet, Mol. Phys. **27**, 1633 (1974).

[3] Y. Iwasaki, K. Maeda, and H. Murai, Time-domain observation of external magnetic field effects on the delayed fluorescence of N,N,N′,N′-Tetramethyl-1,4-phenylenediamine in alcoholic solution, J. Phys. Chem. A **105**, 2961 (2001).

[4] R. Forecast, F. Campaioli, T. W. Schmidt, and J. H. Cole, Photochemical upconversion in solution: The role of oxygen and magnetic field response, J. Phys. Chem. A **127**, 1794 (2023).

[5] M. B. Plenio and S. F. Huelga, Dephasing-assisted transport: quantum networks and biomolecules, New J. Phys. **10**, 113019 (2008).

[6] M. Mohseni, P. Rebentrost, S. Lloyd, and A. Aspuru-Guzik, Environment-assisted quantum walks in photosynthetic energy transfer, J. Chem. Phys. **129**, 174106 (2008).

[7] C. K. Lee, J. Moix, and J. Cao, Coherent quantum transport in disordered systems: A unified polaron treatment of hopping and band-like transport, J. Chem. Phys. **142**, 164103 (2015).

[8] R. Betzholz, J. M. Torres, and M. Bienert, Quantum optical master equation for solid-state quantum emitters, Phys. Rev. A **90**, 063818 (2014).

[9] J. Jeske, D. W. M. Lau, X. Vidal, L. P. McGuinness, P. Reineck, B. C. Johnson, M. W. Doherty, J. C. McCallum, S. Onoda, F. Jelezko, T. Ohshima, T. Volz, J. H. Cole, B. C. Gibson, and A. D. Greentree, Stimulated emission from nitrogen-vacancy centres in diamond, Nat. Commun. **8**, 14000 (2017).

[10] H. Hapuarachchi, F. Campaioli, and J. H. Cole, NV-plasmonics: Modifying optical emission of an NV^- center via plasmonic metal nanoparticles, Nanophotonics **8090**, 1 (2022).

[11] M. Nakano, S. Ito, T. Nagami, Y. Kitagawa, and T. Kubo, Quantum master equation approach to singlet fission dynamics of realistic/artificial pentacene dimer models: Relative relaxation factor analysis, J. Phys. Chem. C **120**, 22803 (2016).

[12] A. Norambuena, A. Jimenez, C. Becher, and J. R. Maze, Effect of phonons on the electron spin resonance absorption spectrum, New J. Phys. **22**, 073068 (2020).

[13] Y. Kobori, M. Fuki, S. Nakamura, and T. Hasobe, Geometries and terahertz motions driving quintet multiexcitons and ultimate triplet–triplet dissociations via the intramolecular singlet fissions, J. Phys. Chem. B **124**, 9411 (2020).

[14] M. I. Collins, F. Campaioli, M. J. Y. Tayebjee, J. H. Cole, and D. R. McCamey, Quintet formation, exchange fluctuations, and the role of stochastic resonance in singlet fission, Commun. Phys. **6**, 1 (2023).

[15] A. G. Redfield, Nuclear magnetic resonance saturation and rotary saturation in solids, Phys. Rev. **98**, 1787 (1955).

[16] J. Hendrickson and P. Bray, A phenomenological equation for NMR motional narrowing in solids, J. Magn. Reson. **9**, 341 (1973).

[17] J. Jeener, A. Vlassenbroek, and P. Broekaert, Unified derivation of the dipolar field and relaxation terms in the Bloch-Redfield equations of liquid NMR, J. Chem. Phys. **103**, 1309 (1998).

[18] M. S. Sarandy and D. A. Lidar, Adiabatic quantum computation in open systems, Phys. Rev. Lett. **95**, 250503 (2005).

[19] F. Verstraete, M. M. Wolf, and J. Ignacio Cirac, Quantum computation and quantum-state engineering driven by dissipation, Nat. Phys. **5**, 633 (2009).

[20] M. Keck, S. Montangero, G. E. Santoro, R. Fazio, and D. Rossini, Dissipation in adiabatic quantum computers: lessons from an exactly solvable model, New J. Phys. **19**, 113029 (2017).

[21] F. Campaioli, C.-s. Yu, F. A. Pollock, and K. Modi, Resource speed limits: Maximal rate of resource variation, New J. Phys. **24**, 065001 (2022).

[22] R. Uzdin, A. Levy, and R. Kosloff, Equivalence of quantum heat machines, and quantum-thermodynamic signatures, Phys. Rev. X **5**, 031044 (2015).

[23] D. Farina, G. M. Andolina, A. Mari, M. Polini, and V. Giovannetti, Charger-mediated energy transfer for quantum batteries: An open-system approach, Phys. Rev. B **99**, 1 (2019).

[24] S. Gherardini, F. Campaioli, F. Caruso, and F. C. Binder, Stabilizing open quantum batteries by sequential measurements, Phys. Rev. Res. **2**, 013095 (2020).

[25] For more on coarse graining and QMEs, see Refs. [69, 109].

[26] H.-P. Breuer and F. Petruccione, *The Theory of Open Quantum Systems* (Oxford University Press, Oxford, 2002).

[27] M. Genkin and E. Lindroth, Description of resonance decay by Lindblad operators, J. Phys. A: Math. Theor. **41**, 425303 (2008).

[28] J. Albers and J. M. Deutch, Redfield—Langevin equation for nuclear spin relaxation, J. Chem. Phys. **55**, 2613 (1971).

[29] F. Campaioli and J. H. Cole, Exciton transport in amorphous polymers and the role of morphology and thermalisation, New J. Phys. **23**, 113038 (2021).

[30] J. R. Johansson, P. D. Nation, and F. Nori, QUTIP: An open-source Python framework for the dynamics of open quantum systems, Comput. Phys. Commun. **183**, 1760 (2012).

[31] H. Chen and D. A. Lidar, Hamiltonian open quantum system toolkit, Commun. Phys. **5**, 1 (2022).

[32] H. Hogben, M. Krzystyniak, G. Charnock, P. Hore, and I. Kuprov, SPINACH — A software library for simulation of spin dynamics in large spin systems, J. Magn. Reson. **208**, 179 (2011).

[33] F. Campaioli, H. Hapuarachchi, and J. H. Cole, See Supplemental Material at http://link.aps.org/supplemental/10.1103/PRXQuantum.5.020202 for a tutorial on quantum master equations: Tips and tricks for quantum optics, quantum computing and beyond.

[34] C. Cohen-Tannoudji, B. Diu, and F. Laloe, *Quantum Mechanics* (Wiley, New York, 1978), Vol. 1.

[35] M. O. Scully and M. S. Zubairy, *Quantum Optics* (Cambridge University Press, Cambridge, 1997).

[36] C. W. Gardiner and P. Zoller, *Quantum Noise* (Springer, Berlin, 2000).

[37] B. H. Bransden and C. J. Joachain, *Quantum Mechanics* (Pearson, Harlow, 2000).

[38] M. A. Schlosshauer, *Decoherence: And the Quantum-To-Classical Transition* (Springer Science and Business Media, Berlin, 2007).

[39] H. M. Wiseman and G. J. Milburn, *Quantum Measurement and Control* (Cambridge University Press, Cambridge, 2009).

[40] U. Weiss, *Quantum Dissipative Systems* (World Scientific, Singapore, 2012).

[41] M. A. Nielsen and I. L. Chuang, *Quantum Computation and Quantum Information: 10th Anniversary Edition* (Cambridge University Press, Cambridge, 2010).

[42] D. McMahon, *Quantum Mechanics Demystified* (McGraw-Hill Education, New York, 2013).

[43] F. Masillo, G. Scolarici, and S. Sozzo, proper versus improper mixtures: Toward a quaternionic quantum mechanics, Theor. Math. Phys. **160**, 1006 (2009).

[44] B. A. Jung and M. Weigel, Spin echo magnetic resonance imaging, J. Magn. Reson. Imaging **37**, 805 (2013).

[45] O. V. Mikhnenko, P. W. Blom, and T. Q. Nguyen, Exciton diffusion in organic semiconductors, Energy Environ. Sci. **8**, 1867 (2015).

[46] T.-C. Wei, K. Nemoto, P. M. Goldbart, P. G. Kwiat, W. J. Munro, and F. Verstraete, Maximal entanglement versus entropy for mixed quantum states, Phys. Rev. A **67**, 022110 (2003).

[47] H.-P. Breuer, Optimal entanglement criterion for mixed quantum states, Phys. Rev. Lett. **97**, 080501 (2006).

[48] F. Mintert, A. R. Carvalho, M. Kuś, and A. Buchleitner, Measures and dynamics of entangled states, Phys. Rep. **415**, 207 (2005).

[49] E. van Nieuwenburg and O. Zilberberg, Entanglement spectrum of mixed states, Phys. Rev. A **98**, 012327 (2018).

[50] Or, more specifically, *positive semidefinite*.

[51] D. Manzano, A short introduction to the Lindblad master equation, AIP Adv. **10**, 025106 (2020).

[52] For example, MATHEMATICA and JULIA use an ordering different from that used by PYTHON.

[53] The state $|\psi(\pi/4)\rangle$ is known as the Φ_+ Bell state [41].

[54] I. Bengtsson and K. Życzkowski, *Geometry of Quantum States: An Introduction to Quantum Entanglement* (Cambridge University Press, Cambridge, 2006).

[55] K. Modi, A. Brodutch, H. Cable, T. Paterek, and V. Vedral, The classical-quantum boundary for correlations: Discord and related measures, Rev. Mod. Phys. **84**, 1655 (2012).

[56] Or the Liouville–von Neumann equation.

[57] C. J. Joachain, *Quantum Collision Theory* (Elsevier, Amsterdam, 1975).

[58] Under some conditions, master equations can also be used beyond the weak-coupling approximation, for example, with the polaron transformation [201] and reaction-coordinate mapping [202].

[59] A. A. Buchheit and G. Morigi, Master equation for high-precision spectroscopy, Phys. Rev. A **94**, 042111 (2016).

[60] M. Authors, in *EPR Spectroscopy: Fundamentals and Methods*, edited by D. Goldfarb and S. Stoll (Wiley, Hoboken, 2018).

[61] A. Kossakowski, On quantum statistical mechanics of non-Hamiltonian systems, Rep. Math. Phys. **3**, 247 (1972).

[62] G. Lindblad, On the generators of quantum dynamical semigroups, Commun. Math. Phys. **48**, 119 (1976).

[63] V. Gorini, A. Kossakowski, and E. C. G. Sudarshan, Completely positive dynamical semigroups of N-level systems, J. Math. Phys. **17**, 821 (2008).

[64] S. Milz, F. A. Pollock, and K. Modi, An Introduction to Operational Quantum Dynamics, Open Syst. Inf. Dyn. **24**, 1740016 (2017).

[65] From now on we drop the subscript S from the system's density operator, unless specified otherwise.

[66] Here we have ignored the effect of Stark and Lamb shift terms, which can appear from the microscopic derivation of the Lindblad master equation. See Refs. [26,69] for more about these terms.

[67] Also known as *collapse* operators or *jump* operators.

[68] Formally, the Lindblad operators are dimensionless linear combinations of the basis operators in Liouville space [26], and therefore the index k in the sum in Eq. (24) can be limited to $d^2 - 1$.

[69] D. A. Lidar, Lecture notes on the theory of open quantum systems, ArXiv:1902.00967.

[70] Column and row ordering are common choices.

[71] S. Barnett, *Matrices: Methods and Applications* (Oxford University Press, Oxford, 1990), Chapter 5.

[72] F. W. Byron and R. W. Fuller, *Mathematics of Classical and Quantum Physics* (Dover Publications, New York, 1992), Chapter 3.

[73] S. Montangero, *Introduction to Tensor Network Methods: Numerical Simulations of Low-Dimensional Many-Body Quantum Systems* (Springer, Berlin, 2018).

[74] R. Orús, A practical introduction to tensor networks: Matrix product states and projected entangled pair states, Ann. Phys. (N. Y.) **349**, 117 (2014).

[75] S. J. Axler, *Linear Algebra Done Right*. Undergraduate Texts in Mathematics (Springer, New York, 1997).

[76] In Sec. V A we outline how to obtain Eq. (32) for a two-level atom interacting with an electric field.

[77] P. D. Nation, Steady-state solution methods for open quantum optical systems, ArXiv:1504.06768.

[78] A nonlinear generator is such that $\mathcal{L}(\rho)$ depends on the state of the system. See Ref. [26] for more on nonlinear density operator master equations.

[79] S. Stenholm and K.-A. Suominen, *Quantum Approach to Informatics* (John Wiley & Sons, Hoboken, 2005).

[80] P. Lambropoulos and D. Petrosyan, *Fundamentals of Quantum Optics and Quantum Information* (Springer Berlin, Heidelberg, Berlin, 2007).

[81] S. Kim and F. Hassler, Third quantization for bosons: symplectic diagonalization, non-Hermitian Hamiltonian, and symmetries, J. Phys. A: Math. Theor. **56**, 385303 (2023).

[82] A generalization of the eigenvalue decomposition.

[83] A tensor $A_{i_1,\ldots,i_m j_1\ldots j_m}$ is Hermitian if $A_{i_1,\ldots,i_m j_1\ldots j_m} = A^*_{j_1,\ldots,j_m i_1\ldots i_m}$ for all indices, where $*$ is the complex conjugation [203].

[84] K. Sacha, in *Time Crystals* (Springer International Publishing, 2020), p. 39.

[85] F. Minganti, A. Biella, N. Bartolo, and C. Ciuti, Spectral theory of Liouvillians for dissipative phase transitions, Phys. Rev. A **98**, 042118 (2018).

[86] W. Rossmann, *Lie Groups: An Introduction Through Linear Groups* (Oxford University Press, Oxford, 2002).

[87] For most physical systems the superoperator $\mathcal{L}$ is sparse, so its memory complexity scales not as d^4 but rather as $d^2 2\log(d)$ (see Sec. III D 8 for more on methods for sparse superoperators).

[88] A. Bortz, M. Kalos, and J. Lebowitz, A new algorithm for Monte Carlo simulation of Ising spin systems, J. Comput. Phys. **17**, 10 (1975).

[89] I. Yusipov, T. Laptyeva, S. Denisov, and M. Ivanchenko, Localization in open quantum systems, Phys. Rev. Lett. **118**, 070402 (2017).

[90] F. Vicentini, F. Minganti, A. Biella, G. Orso, and C. Ciuti, Optimal stochastic unraveling of disordered open quantum systems: Application to driven-dissipative photonic lattices, Phys. Rev. A **99**, 032115 (2019).

[91] The method can be implemented with non-Hermitian Lindblad operators too, upon some adaptations to avoid division-by-zero errors in the normalization steps.

[92] A. Schnell, A. Eckardt, and S. Denisov, Is there a Floquet Lindbladian?, Phys. Rev. B **101**, 100301 (2020).

[93] T. A. Davis, *Direct Methods for Sparse Linear Systems* (SIAM, Philadelphia, 2006).

[94] H. D. Vo and R. B. Sidje, Approximating the large sparse matrix exponential using incomplete orthogonalization and Krylov subspaces of variable dimension, Numer. Linear Algebra Appl. **24**, e2090 (2017).

[95] A. Gaul, Recycling Krylov subspace methods for sequences of linear systems: Analysis and applications, Doctoral thesis, Technische Universität Berlin, Fakultät II—Mathematik und Naturwissenschaften, Berlin, 2014.

[96] M. Knap, E. Arrigoni, W. von der Linden, and J. H. Cole, Emission characteristics of laser-driven dissipative coupled-cavity systems, Phys. Rev. A **83**, 023821 (2011).

[97] F. Minganti and D. Huybrechts, Arnoldi-Lindblad time evolution: Faster-than-the-clock algorithm for the spectrum of time-independent and Floquet open quantum systems, Quantum **6**, 649 (2022).

[98] C. Paterson, Atmospheric turbulence and orbital angular momentum of single photons for optical communication, Phys. Rev. Lett. **94**, 153901 (2005).

[99] M. C. Gutzwiller, Effect of correlation on the ferromagnetism of transition metals, Phys. Rev. Lett. **10**, 159 (1963).

[100] M. Hennrich, A. Kuhn, and G. Rempe, Transition from antibunching to bunching in cavity QED, Phys. Rev. Lett. **94**, 053604 (2005).

[101] C. Emary, C. Pöltl, A. Carmele, J. Kabuss, A. Knorr, and T. Brandes, Bunching and antibunching in electronic transport, Phys. Rev. B **85**, 165417 (2012).

[102] Z. Ficek and S. Swain, *Quantum Interference and Coherence: Theory and Experiments* (Springer Science & Business Media, Berlin, 2005), Vol. 100.

[103] C. Gardiner, P. Zoller, and P. Zoller, *Quantum Noise: A Handbook of Markovian and Non-Markovian Quantum Stochastic Methods with Applications to Quantum Optics* (Springer Science & Business Media, Berlin, 2004).

[104] P. Zhou and S. Swain, Absorption spectrum of a two-level atom in a bad cavity with injected squeezed vacuum, Opt. Commun. **131**, 153 (1996).

[105] R. Tanas and T. El-Shahat, Analytical results for the probe absorption spectrum of a driven two-level atom in a squeezed vacuum with finite bandwidth, Acta Phys. Slovaca **48**, 301 (1998).

[106] Z. Xu, S. Xie, S.-Y. Zhu, and M. O. Scully, *Frontiers of Laser Physics and Quantum Optics: Proceedings of the International Conference on Laser Physics and Quantum Optics* (Springer Science & Business Media, Berlin, 2013).

[107] P. Meystre and M. Sargent, *Elements of Quantum Optics* (Springer Science & Business Media, Berlin, 2007).

[108] P. D. Nation and J. Johansson, Quantum Toolbox in Python, available online at http://qutip.org (2011).

[109] C. Cohen-Tannoudji, G. Grynberg, and J. Dupont-Roc, *Atom-Photon Interactions: Basic Processes and Applications* (Wiley, New York, 1992).

[110] $H_S|\omega_a\rangle = \hbar\omega_a|\omega_a\rangle$.

[111] P. W. Jones and P. Smith, *Stochastic Processes: An Introduction* (CRC Press, Cambridge, 2017), 3rd ed.

[112] A. W. Chin, Á. Rivas, S. F. Huelga, and M. B. Plenio, Exact mapping between system-reservoir quantum models and semi-infinite discrete chains using orthogonal polynomials, J. Math. Phys. **51**, 092109 (2010).

[113] See Sec. II for definition and properties and completely positive and trace-preserving maps.

[114] R. S. Whitney, Staying positive: Going beyond Lindblad with perturbative master equations, J. Phys. A: Math. Theor. **41**, 175304 (2008).

[115] H. Mäkelä and M. Möttönen, Effects of the rotating-wave and secular approximations on non-Markovianity, Phys. Rev. A **88**, 052111 (2013).

[116] S. J. Jang and B. Mennucci, Delocalized excitons in natural light-harvesting complexes, Rev. Mod. Phys. **90**, 035003 (2018).

[117] A. Strathearn, P. Kirton, D. Kilda, J. Keeling, and B. W. Lovett, Efficient non-Markovian quantum dynamics using time-evolving matrix product operators, Nat. Commun. **9**, 1 (2018).

[118] I. Kondov, U. Kleinekathöfer, and M. Schreiber, Efficiency of different numerical methods for solving Redfield equations, J. Chem. Phys. **114**, 1497 (2001).

[119] C. Moler and C. Van Loan, Nineteen dubious ways to compute the exponential of a matrix, twenty-five years later, SIAM Rev. **45**, 3 (2003).

[120] A. H. Al-Mohy and N. J. Higham, A new scaling and squaring algorithm for the matrix exponential, SIAM J. Matrix Anal. Appl. **31**, 970 (2010).

[121] J. Jeske, D. J. Ing, M. B. Plenio, S. F. Huelga, and J. H. Cole, Bloch-Redfield equations for modeling light-harvesting complexes, J. Chem. Phys. **142**, 064104 (2015).
[122] S. Davidson, A. Fruchtman, F. A. Pollock, and E. M. Gauger, The dark side of energy transport along excitonic wires: On-site energy barriers facilitate efficient, vibrationally mediated transport through optically dark subspaces, J. Chem. Phys. **153**, 134701 (2020).
[123] S. Davidson, F. A. Pollock, and E. Gauger, Eliminating radiative losses in long-range exciton transport, Phys. Rev. X Quantum **3**, 020354 (2022).
[124] D. A. Steck, Quantum and atom optics, http://www.nadirpoint.de/Physik_Lit_PDF/62.pdf (2007).
[125] R. D. Artuso, The Optical Response of Strongly Coupled Quantum Dot-Metal Nanoparticle Hybrid Systems, Ph.D. thesis, University of Maryland, College Park, Maryland, United States, 2012, available online at https://drum.lib.umd.edu/handle/1903/13644.
[126] M. Scala, B. Militello, A. Messina, S. Maniscalco, J. Piilo, and K.-A. Suominen, Cavity losses for the dissipative Jaynes–Cummings Hamiltonian beyond rotating wave approximation, J. Phys. A: Math. Theor. **40**, 14527 (2007).
[127] J. H. Shirley, Solution of the Schrödinger equation with a Hamiltonian periodic in time, Phys. Rev. **138**, B979 (1965).
[128] O. Kyriienko and A. S. Sørensen, Floquet quantum simulation with superconducting qubits, Phys. Rev. Appl. **9**, 064029 (2018).
[129] R. W. Bomantara and J. Gong, Quantum computation via Floquet topological edge modes, Phys. Rev. B **98**, 165421 (2018).
[130] S. Restrepo, J. Cerrillo, P. Strasberg, and G. Schaller, From quantum heat engines to laser cooling: Floquet theory beyond the Born–Markov approximation, New J. Phys. **20**, 053063 (2018).
[131] B. Bartels and F. Mintert, Smooth optimal control with Floquet theory, Phys. Rev. A **88**, 052315 (2013).
[132] A. Castro, U. De Giovannini, S. A. Sato, H. Hübener, and A. Rubio, Floquet engineering the band structure of materials with optimal control theory, Phys. Rev. Res. **4**, 033213 (2022).
[133] D. V. Else, B. Bauer, and C. Nayak, Floquet time crystals, Phys. Rev. Lett. **117**, 090402 (2016).
[134] K. Sacha and J. Zakrzewski, Time crystals: A review, Rep. Prog. Phys. **81**, 016401 (2017).
[135] C. Creffield, Location of crossings in the Floquet spectrum of a driven two-level system, Phys. Rev. B **67**, 165301 (2003).
[136] H.-P. Breuer, W. Huber, and F. Petruccione, Quasistationary distributions of dissipative nonlinear quantum oscillators in strong periodic driving fields, Phys. Rev. E **61**, 4883 (2000).
[137] B. H. Wu and C. Timm, Noise spectra of ac-driven quantum dots: Floquet master-equation approach, Phys. Rev. B **81**, 075309 (2010).
[138] T. Mori, Floquet states in open quantum systems, Annu. Rev. Condens. Matter Phys. **14**, 35 (2023).
[139] T. Werlang, A. V. Dodonov, E. I. Duzzioni, and C. J. Villas-Bôas, Rabi model beyond the rotating-wave approximation: Generation of photons from vacuum through decoherence, Phys. Rev. A **78**, 053805 (2008).
[140] C. Majenz, T. Albash, H.-P. Breuer, and D. A. Lidar, Coarse graining can beat the rotating-wave approximation in quantum Markovian master equations, Phys. Rev. A **88**, 012103 (2013).
[141] C. Müller and T. M. Stace, Deriving Lindblad master equations with Keldysh diagrams: Correlated gain and loss in higher order perturbation theory, Phys. Rev. A **95**, 013847 (2017).
[142] S. Kohler, Dispersive readout: Universal theory beyond the rotating-wave approximation, Phys. Rev. A **98**, 023849 (2018).
[143] A. D. Bain and R. S. Dumont, Introduction to Floquet theory: The calculation of spinning sideband intensities in magic-angle spinning NMR, Concepts Magn. Reson. **13**, 159 (2001).
[144] P. Bushev, C. Müller, J. Lisenfeld, J. H. Cole, A. Lukashenko, A. Shnirman, and A. V. Ustinov, Multiphoton spectroscopy of a hybrid quantum system, Phys. Rev. B **82**, 134530 (2010).
[145] Y. Schön, J. N. Voss, M. Wildermuth, A. Schneider, S. T. Skacel, M. P. Weides, J. H. Cole, H. Rotzinger, and A. V. Ustinov, Rabi oscillations in a superconducting nanowire circuit, npj Quantum Mater. **5**, 1 (2020).
[146] F. Benatti and R. Floreanini, *Direct Methods for Sparse Linear Systems* (Springer, Berlin, 2003).
[147] A. Rivas and F. S. Huelga, *Open Quantum Systems* (Springer, Berlin, 2012).
[148] Y. Tanimura, Stochastic Liouville, Langevin, Fokker–Planck, and master equation approaches to quantum dissipative systems, J. Phys. Soc. Jpn. **75**, 082001 (2006).
[149] I. Rotter and J. P. Bird, A review of progress in the physics of open quantum systems: Theory and experiment, Rep. Prog. Phys. **78**, 114001 (2015).
[150] H.-P. Breuer, E.-M. Laine, J. Piilo, and B. Vacchini, *Colloquium*: Non-Markovian dynamics in open quantum systems, Rev. Mod. Phys. **88**, 021002 (2016).
[151] T. Yu, L. Diósi, N. Gisin, and W. T. Strunz, Non-Markovian quantum-state diffusion: Perturbation approach, Phys. Rev. A **60**, 91 (1999).
[152] H.-P. Breuer, B. Kappler, and F. Petruccione, Stochastic wave-function method for non-Markovian quantum master equations, Phys. Rev. A **59**, 1633 (1999).
[153] T. Yu, Non-Markovian quantum trajectories versus master equations: Finite-temperature heat bath, Phys. Rev. A **69**, 062107 (2004).
[154] L. Ferialdi, Exact closed master equation for Gaussian non-Markovian dynamics, Phys. Rev. Lett. **116**, 120402 (2016).
[155] J. Piilo, S. Maniscalco, K. Härkönen, and K.-A. Suominen, Non-Markovian quantum jumps, Phys. Rev. Lett. **100**, 180402 (2008).
[156] W.-M. Zhang, Exact master equation and general non-Markovian dynamics in open quantum systems, Eur. Phys. J. Spec. Top. **227**, 1849 (2019).

[157] S. Ya Kilin and A. P. Nizovtsev, Generalised non-linear optical master equations taking into account the correlation time of relaxational perturbations, J. Phys. B: At., Mol., Phys. **19**, 3457 (1986).
[158] T. Mančal and F. Šanda, Quantum master equations for non-linear optical response of molecular systems, Chem. Phys. Lett. **530**, 140 (2012).
[159] A. Pereverzev and E. R. Bittner, Time-convolutionless master equation for mesoscopic electron-phonon systems, J. Chem. Phys. **125**, 104906 (2006).
[160] G. Nan, Q. Shi, and Z. Shuai, Nonperturbative time-convolutionless quantum master equation from the path integral approach, J. Chem. Phys. **130**, 134106 (2009).
[161] C. Timm, Time-convolutionless master equation for quantum dots: Perturbative expansion to arbitrary order, Phys. Rev. B **83**, 115416 (2011).
[162] L. Kidon, E. Y. Wilner, and E. Rabani, Exact calculation of the time convolutionless master equation generator: Application to the nonequilibrium resonant level model, J. Chem. Phys. **143**, 234110 (2015).
[163] P.-Y. Yang and W.-M. Zhang, Master equation approach to transient quantum transport in nanostructures, Front. Phys. **12**, 127204 (2016).
[164] D. Brian and X. Sun, Generalized quantum master equation: A tutorial review and recent advances, Chin. J. Chem. Phys. **34**, 497 (2021).
[165] M. S. Ferguson, O. Zilberberg, and G. Blatter, Open quantum systems beyond Fermi's golden rule: Diagrammatic expansion of the steady-state time-convolutionless master equations, Phys. Rev. Res. **3**, 023127 (2021).
[166] S. L. Wu and W. Ma, Trajectory tracking for non-Markovian quantum systems, Phys. Rev. A **105**, 012204 (2022).
[167] D. Davidović, Geometric-arithmetic master equation in large and fast open quantum systems, J. Phys. A: Math. Theor. **55**, 455301 (2022).
[168] B. Donvil and P. Muratore-Ginanneschi, Quantum trajectory framework for general time-local master equations, Nat. Commun. **13**, 4140 (2022).
[169] P. Stenius and A. Imamoglu, Stochastic wavefunction methods beyond the Born - Markov and rotating-wave approximations, Quantum Semiclassical Opt.: J. Eur. Opt. Soc. B **8**, 283 (1996).
[170] D. Davidović, Completely positive, simple, and possibly highly accurate approximation of the redfield equation, Quantum **4**, 326 (2020).
[171] M. Cygorek, M. Cosacchi, A. Vagov, V. M. Axt, B. W. Lovett, J. Keeling, and E. M. Gauger, Simulation of open quantum systems by automated compression of arbitrary environments, Nat. Phys. **18**, 662 (2022).
[172] A. H. Werner, D. Jaschke, P. Silvi, M. Kliesch, T. Calarco, J. Eisert, and S. Montangero, Positive tensor network approach for simulating open quantum many-body systems, Phys. Rev. Lett. **116**, 237201 (2016).
[173] X. Xu, J. Thingna, C. Guo, and D. Poletti, Many-body open quantum systems beyond Lindblad master equations, Phys. Rev. A **99**, 012106 (2019).
[174] M. R. Jørgensen and F. A. Pollock, Exploiting the causal tensor network structure of quantum processes to efficiently simulate non-Markovian path integrals, Phys. Rev. Lett. **123**, 240602 (2019).
[175] D. M. Fugger, D. Bauernfeind, M. E. Sorantin, and E. Arrigoni, Nonequilibrium pseudogap Anderson impurity model: A master equation tensor network approach, Phys. Rev. B **101**, 165132 (2020).
[176] H. Nakano, T. Shirai, and T. Mori, Tensor network approach to thermalization in open quantum many-body systems, Phys. Rev. E **103**, L040102 (2021).
[177] Numerical implementations of these methods are available in libraries such as ITensor [204] and Quantum TEA [205].
[178] F. Vicentini, A. Biella, N. Regnault, and C. Ciuti, Variational neural-network ansatz for steady states in open quantum systems, Phys. Rev. Lett. **122**, 250503 (2019).
[179] M. J. Hartmann and G. Carleo, Neural-network approach to dissipative quantum many-body dynamics, Phys. Rev. Lett. **122**, 250502 (2019).
[180] Z. Liu, L.-M. Duan, and D.-L. Deng, Solving quantum master equations with deep quantum neural networks, Phys. Rev. Res. **4**, 013097 (2022).
[181] Numerical implementations of neural-network methods for many-body quantum systems are available in the open-source PYTHON library NetKet [206,207].
[182] R. Di Candia, J. S. Pedernales, A. del Campo, E. Solano, and J. Casanova, Quantum simulation of dissipative processes without reservoir engineering, Sci. Rep. **5**, 9981 (2015).
[183] S. Endo, J. Sun, Y. Li, S. C. Benjamin, and X. Yuan, Variational quantum simulation of general processes, Phys. Rev. Lett. **125**, 010501 (2020).
[184] A. W. Schlimgen, K. Head-Marsden, L. M. Sager, P. Narang, and D. A. Mazziotti, Quantum simulation of the Lindblad equation using a unitary decomposition of operators, Phys. Rev. Res. **4**, 023216 (2022).
[185] H. Kamakari, S.-N. Sun, M. Motta, and A. J. Minnich, Digital quantum simulation of open quantum systems using quantum imaginary–time evolution, PRX Quantum **3**, 010320 (2022).
[186] G. D. Chiara and A. Sanpera, Genuine quantum correlations in quantum many-body systems: A review of recent progress, Rep. Prog. Phys. **81**, 074002 (2018).
[187] M. Heyl, Dynamical quantum phase transitions: A brief survey, Europhys. Lett. **125**, 26001 (2019).
[188] L. Bayha, M. Holten, R. Klemt, K. Subramanian, J. Bjerlin, S. M. Reimann, G. M. Bruun, P. M. Preiss, and S. Jochim, Observing the emergence of a quantum phase transition shell by shell, Nature **587**, 583 (2020).
[189] A. Carollo, D. Valenti, and B. Spagnolo, Geometry of quantum phase transitions, Phys. Rep. **838**, 1 (2020).
[190] D. Rossini and E. Vicari, Coherent and dissipative dynamics at quantum phase transitions, Phys. Rep. **936**, 1 (2021).
[191] X. Wu, X. Liang, Y. Tian, F. Yang, C. Chen, Y.-C. Liu, M. K. Tey, and L. You, A concise review of Rydberg atom based quantum computation and quantum simulation, Chin. Phys. B **30**, 020305 (2021).
[192] K. R. Brown, J. Chiaverini, J. M. Sage, and H. Häffner, Materials challenges for trapped-ion quantum computers, Nat. Rev. Mater. **6**, 892 (2021).
[193] S. Bravyi, O. Dial, J. M. Gambetta, D. Gil, and Z. Nazario, The future of quantum computing with superconducting qubits, J. Appl. Phys. **132**, 160902 (2022).

[194] L. S. Madsen, F. Laudenbach, M. F. Askarani, F. Rortais, T. Vincent, J. F. F. Bulmer, F. M. Miatto, L. Neuhaus, L. G. Helt, M. J. Collins, A. E. Lita, T. Gerrits, S. W. Nam, V. D. Vaidya, M. Menotti, I. Dhand, Z. Vernon, N. Quesada, and J. Lavoie, Quantum computational advantage with a programmable photonic processor, Nature **606**, 75 (2022).

[195] A. Chenu and G. D. Scholes, Coherence in energy transfer and photosynthesis, Annu. Rev. Phys. Chem. **66**, 69 (2015).

[196] G. D. Scholes, Polaritons and excitons: Hamiltonian design for enhanced coherence, Proc. R. Soc. A: Math. Phys. Eng. Sci. **476**, 20200278 (2020).

[197] Y. Cao, J. Romero, J. P. Olson, M. Degroote, P. D. Johnson, M. Kieferová, I. D. Kivlichan, T. Menke, B. Peropadre, N. P. D. Sawaya, S. Sim, L. Veis, and A. Aspuru-Guzik, Quantum chemistry in the age of quantum computing, Chem. Rev. **119**, 10856 (2019).

[198] F. A. Schröder, D. H. Turban, A. J. Musser, N. D. Hine, and A. W. Chin, Tensor network simulation of multi-environmental open quantum dynamics via machine learning and entanglement renormalisation, Nat. Commun. **10**, 1 (2019).

[199] S. McArdle, S. Endo, A. Aspuru-Guzik, S. C. Benjamin, and X. Yuan, Quantum computational chemistry, Rev. Mod. Phys. **92**, 015003 (2020).

[200] E. Ye and G. K. L. Chan, Constructing tensor network influence functionals for general quantum dynamics, J. Chem. Phys. **155**, 044104 (2021).

[201] N. A. Deskins and M. Dupuis, Electron transport via polaron hopping in bulk TiO_2: A density functional theory characterization, Phys. Rev. B: Condens. Matter Mater. Phys. **75**, 1 (2007).

[202] J. Iles-Smith, N. Lambert, and A. Nazir, Environmental dynamics, correlations, and the emergence of noncanonical equilibrium states in open quantum systems, Phys. Rev. A **90**, 032114 (2014).

[203] G. Ni, Hermitian tensor and quantum mixed state, ArXiv:1902.02640.

[204] M. Fishman, S. R. White, and E. M. Stoudenmire, The ITensor software library for tensor network calculations, SciPost Phys. Codebases **4** (2022).

[205] Quantum Tea, Quantum tensor-network emulator applications, https://baltig.infn.it/quantum_tea (2022), accessed 2023-04-24.

[206] G. Carleo, K. Choo, D. Hofmann, J. E. T. Smith, T. Westerhout, F. Alet, E. J. Davis, S. Efthymiou, I. Glasser, S.-H. Lin, M. Mauri, G. Mazzola, C. B. Mendl, E. van Nieuwenburg, O. O'Reilly, H. Théveniaut, G. Torlai, F. Vicentini, and A. Wietek, NetKet: A machine learning toolkit for many-body quantum systems, SoftwareX **10**, 100311 (2019).

[207] F. Vicentini, D. Hofmann, A. Szabó, D. Wu, C. Roth, C. Giuliani, G. Pescia, J. Nys, V. Vargas-Calderón, N. Astrakhantsev, and G. Carleo, NetKet 3: Machine learning toolbox for many-body quantum systems, SciPost Phys. Codebases **7**, 7 (2022).